Computing Voronoi Diagrams in the Polar-Coordinate Model of the Hyperbolic Plane

Tobias Friedrich
Hasso Plattner Institute, University of Potsdam
Potsdam, Germany

Maximilian Katzmann
Karlsruhe Institute of Technology
Karlsruhe, Germany

Leon Schiller
Hasso Plattner Institute, University of Potsdam
Potsdam, Germany

arXiv:2112.02553v2 [cs.CG] 26 Jan 2023

Abstract

A Voronoi diagram is a basic geometric structure that partitions the space into regions associated with a given set of sites, such that all points in a region are closer to the corresponding site than to all other sites. While being thoroughly studied in Euclidean space, they are also of interest in hyperbolic space. In fact, there are several algorithms for computing hyperbolic Voronoi diagrams that work with the various models used to describe hyperbolic geometry. However, the *polar-coordinate model* has not been considered before, despite its popularity in the network science community. While Voronoi diagrams have the potential to advance this field, the model is geometrically not as approachable as other models, which impedes the development of geometric algorithms.

In this paper, we present an algorithm for computing Voronoi diagrams natively in the polar-coordinate model of the hyperbolic plane. The approach is based on Fortune's sweep line algorithm for Euclidean Voronoi diagrams. We characterize the hyperbolic counterparts of the concepts it utilizes and introduce adaptations necessary to account for the differences.

We implemented our algorithm and compared it with the corresponding CGAL implementation. While not being as numerically stable, our method has proven to be useful as a reference, which helped resolving fundamental issues in the implementation of the state-of-the-art method.

2012 ACM Subject Classification Theory of computation → Computational geometry; Theory of computation → Data structures design and analysis

Keywords and phrases Voronoi diagram, hyperbolic geometry, sweep line algorithm, delaunay complex, hyperbolic random graphs

1 Introduction

The Voronoi diagram is a fundamental and well-studied geometric structure. Given a set of points, which we call *sites*, the goal is to partition the space into *cells*, i.e., regions that are associated with the sites, such that no site is closer to a point in a cell than the associated one. Typically, the sites are assumed to lie in Euclidean space, where finding the Voronoi diagram or its geometric dual, the Delaunay triangulation, has various applications in biology, computer graphics, and robotics [5, 12, 17]. However, this problem is also relevant in hyperbolic geometry, in the context of finding certain Möbius transformations [2], computing Delaunay triangulations of points in two planes [9], or for greedy routing in networks [34].

Hyperbolic and Euclidean geometry differ in several fundamental properties. First, space expands exponentially fast in hyperbolic space, while the expansion is only polynomial in Euclidean space. Second, for a hyperbolic line there are infinitely many lines that go through a point not on the line and are parallel to the first one. And, third, in contrast to the flat Euclidean space, hyperbolic space is negatively curved.

Over time, various models have been developed to capture these properties and facilitate the study of hyperbolic geometry. While some models, like the *Poincaré ball*, the *Klein ball*, and the *hemisphere model* represent the infinite hyperbolic space in a finite region in Euclidean space, other models like the *upper-half-plane model* and the *hyperboloid model* map it onto unbounded Euclidean regions. For an overview we refer the reader to [31, Chapter 7].

With the different models came different approaches to computing Voronoi diagrams. For the upper-half-plane model there is an algorithm that computes it from a Euclidean one [30]. A similar approach was later used to generalize an $\mathcal{O}(n^2)$-algorithm in the Poincaré disk [29], to an $\mathcal{O}(n \log(n))$-algorithm in the Poincaré ball [6]. Another method is based on power diagrams and utilizes the Klein disk model [27]. We refer the reader to [34] for an overview of hyperbolic Voronoi diagrams, to [26] for their relation to hyperbolic Delaunay complexes, and to [28] for visualizations in different models. We note that converting between the various representations typically involves scaling the coordinates exponentially, which can lead to numerical issues. Consequently, it is best to perform all computations directly in one model, instead of taking detours through other representations.

A model that has not been considered in the context of hyperbolic Voronoi diagrams before is the *polar-coordinate model*, which is rather surprising given its popularity in the study of complex networks. There, the polar-coordinate representation is used to analyze real-world networks like protein-interaction networks, the internet, and trade networks [1, 8, 16]. In particular, *hyperbolic random graphs*, a generative graph model aimed at representing such networks, were introduced using the polar-coordinate model of the hyperbolic plane [22], and it was since shown that this representation is particularly well-suited for mathematical analysis of network properties and algorithms [3, 4, 18, 23, 25]. Being able to compute Voronoi diagrams in this model has the potential to further advance this field.

One reason for the mathematical accessibility of the polar-coordinate model is its straightforward definition. Points in hyperbolic space are addressed using their distance to a dedicated point, called *pole*, and the angular distance to a ray starting at the pole, called *polar axis*. The resulting coordinates are then simply interpreted as polar coordinates in Euclidean space. However, in contrast to models like the Poincaré disk, where hyperbolic circles are Euclidean circles (with offset centers) and hyperbolic lines are circular arcs in Euclidean space, or the hyperboloid model, where hyperbolic circles and lines are intersections of planes with the hyperboloid, the polar-coordinate model is not as approachable from a geometric point of view. There, hyperbolic circles are shaped like tear drops and lines are hyperbolas that are

bent towards the pole (see Figure 1 (left) for an illustration). As a consequence, this model has not been considered in the context of geometric algorithms before.

In this paper, we present an algorithm for computing Voronoi diagrams directly in the polar-coordinate model of the two-dimensional hyperbolic plane. The approach is based on Fortune's sweep line algorithm for solving the problem in the Euclidean plane [13], which scans the plane and maintains data structures to incrementally build the diagram using a so-called *beach line*. More precisely, our approach builds on a generalization of Fortune's algorithm that uses an expanding sweep circle instead of a line [35], while maintaining an optimal running time of $\mathcal{O}(n \log(n))$.

The resulting algorithm is simple and while proving its correctness follows known techniques, we note that translating them to work with the considered model of hyperbolic geometry is not trivial. In contrast, prior work nicely demonstrates that other models allow for utilizing parallels to Euclidean geometry (see, e.g., [6, 30]), yet the resulting algorithms are more complicated and thus harder to implement.

We implemented our algorithm and compared it to the state-of-the-art method for computing hyperbolic Voronoi diagrams and Delaunay complexes [6], which is available in CGAL [7]. Since this method works with the Poincaré disk model of the hyperbolic plane, utilizing it for our purposes requires converting between the Poincaré disk and the polar-coordinate model. Surprisingly, our results show that the computation of the Voronoi vertices is more reliable than in our native approach, despite these conversions. However, further comparisons with our method showed that the CGAL implementation was not able to reliably compute the correct structure of the diagram. In fact, adjacent Voronoi cells were often not detected as such (corresponding to missing edges in the Delaunay triangulation). After reporting the issue[1], it turned out that solving it required a sizable change in the implementation[2], which highlights the usefulness of reference implementations that are based on simple algorithms. Beyond that, we observe that both methods suffer from numerical inaccuracies. Thus, while our method represents the first step towards utilizing geometric algorithms in the polar-coordinate model of the hyperbolic plane, further research is necessary to obtain scalable methods.

We note that proofs and in particular the proof of correctness and running time analysis of our algorithm are deferred to Appendix A.

2 Preliminaries

We denote points with capital letters like P, Q and sets or tuples with calligraphic capital letters like $\mathcal{S}, \mathcal{V}$. Given two points P, Q, we denote the line through them with $\overleftrightarrow{PQ}$ and the ray from P through Q with $\overrightarrow{PQ}$. A ray starting at P, whose direction is given by context is denoted by $\overrightarrow{P}$. The line segment between P and Q is written as $\overline{PQ}$ and $|\overline{PQ}|$ denotes its length, i.e., the distance between P and Q. The *perpendicular bisector*, i.e., the set of points with equal distance to P and Q is denoted by $P \perp Q$. A *circle* with center P, i.e., the set of all points Q with equal distance to P is denoted by $\odot P$ (its radius is given by context). The points Q are said to lie on the *arc* of $\odot P$. Triangles are written as $\triangle PQS$ and $\sphericalangle PQS$ denotes the angle between $\overrightarrow{QP}$ and $\overrightarrow{QS}$ measured in *clockwise* direction around Q. The intersection of two objects is denoted with a $\cap$-sign.

[1] https://github.com/CGAL/cgal/issues/6869
[2] https://github.com/MaelRL/cgal/commit/cf12f90cbf721fbbf6752d98c6d76190b6a5052c

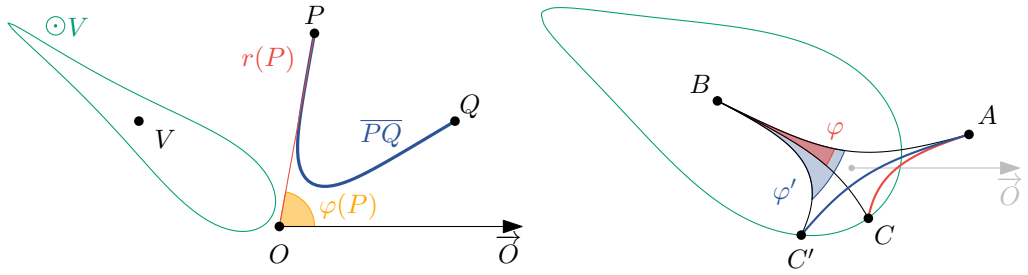


Figure 1 (Left) The polar-coordinate model of the hyperbolic plane. The line segment $\overline{PQ}$ is shown in blue. Point V is the center of the tear-drop shaped green circle $\odot V$. **(Right)** Illustration of the triangles $\triangle ABC$ and $\triangle ABC'$ from Lemma 1. Since C and C' lie on a circle (green) with center B, we have $|\overline{BC}| = |\overline{BC'}|$. When increasing the angle φ at B to φ' then $|\overline{AC}| < |\overline{AC'}|$.

The Hyperbolic Plane. In this paper, we work with the *polar-coordinate model* of the hyperbolic plane $\mathbb{H}^2$. There, points are identified using polar coordinates. After defining a designated *origin* or *pole* $O \in \mathbb{H}^2$ together with a *polar axis* $\overrightarrow{O}$, i.e., a reference ray starting at O, a point $P \in \mathbb{H}^2$ is identified using its *radius* $r(P)$ denoting the hyperbolic distance to O and its *angle* $\varphi(P)$ denoting the angular distance to $\overrightarrow{O}$ in counterclockwise direction around O. For visualizations, these coordinates are then interpreted as polar coordinates in the Euclidean plane, as shown in Figure 1. We note that angles at line intersections are *not* preserved by the representation and are only added in our figures for illustration purposes.

In contrast to Euclidean geometry, the sum of the angles in a triangle $\triangle ABC$ is strictly less than π in the hyperbolic plane. Still, we can relate the length of $\overline{AB}$ to the lengths of the other segments and the angle φ at C, via the *hyperbolic law of cosines*, which is defined as

$$\cosh(|\overline{AB}|) = \cosh(|\overline{AC}|)\cosh(|\overline{BC}|) - \sinh(|\overline{AC}|)\sinh(|\overline{BC}|)\cos(\varphi), \tag{1}$$

where $\sinh(x) = (e^x - e^{-x})/2$, $\cosh(x) = (e^x + e^{-x})/2$. Analogous to Euclidean geometry, the hyperbolic tangent tanh is defined as the quotient of the hyperbolic sine and cosine. We denote the inverse hyperbolic trigonometric functions with asinh, acosh, and atanh. Note that we can use the hyperbolic law of cosines to derive the distance between $A, B \in \mathbb{H}^2$ by considering the triangle $\triangle AOB$, where the angle at O is $\varphi = \Delta_\varphi(A, B) = \pi - |\pi - |\varphi(A) - \varphi(B)||$. Since $\cos(\pi - x) = -\cos(x)$ and $\cos(-x) = \cos(x)$, we have $\cos(\Delta_\varphi(A, B)) = \cos(\varphi(A) - \varphi(B))$. Thus, the hyperbolic distance between A and B is given by

$$|\overline{AB}| = \operatorname{acosh}\big(\cosh(r(A))\cosh(r(B)) - \sinh(r(A))\sinh(r(B))\cos(\varphi(A) - \varphi(B))\big). \tag{2}$$

The distance between a circle of radius r centered at the pole and a point A with radius $r(A) \leq r$ is given by $r - r(A)$. The following lemma shows that changing an angle in a triangle also changes the length of the opposite line segment, as illustrated in Figure 1 (right).

▶ **Lemma 1.** *Let $\triangle ABC$ and $\triangle ABC'$ be triangles with $|\overline{BC}| = |\overline{BC'}|$ and angles φ and φ' at B, respectively. Then, $\varphi < \varphi'$ (resp. $\varphi > \varphi'$) if and only if $|\overline{AC}| < |\overline{AC'}|$ (resp. $|\overline{AC}| > |\overline{AC'}|$).*

We note that in a degenerate triangle where the angle at B is π, the length of the segment opposite of B is given by the sum of the lengths of the other two segments. Thus, the above lemma confirms the fact that the triangle inequality also holds in the hyperbolic plane. The following lemma shows that, if two points B, C have certain distances to a third point A, then every distance between the two distances is realized by a point on $\overline{BC}$.

▶ **Lemma 2.** *Let $\triangle ABC$ be a triangle with $|\overline{AB}| \leq |\overline{AC}|$. For every $d \in [|\overline{AB}|, |\overline{AC}|]$, there exists a point $P \in \overline{BC}$ with $|\overline{AP}| = d$.*

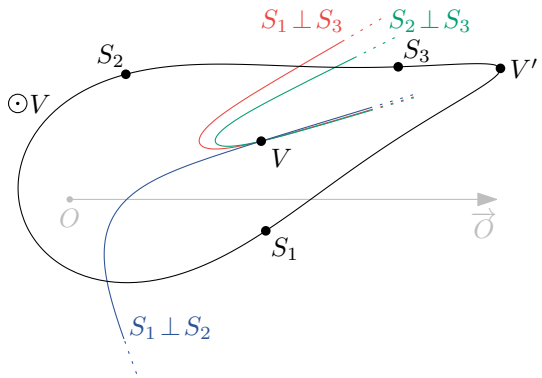


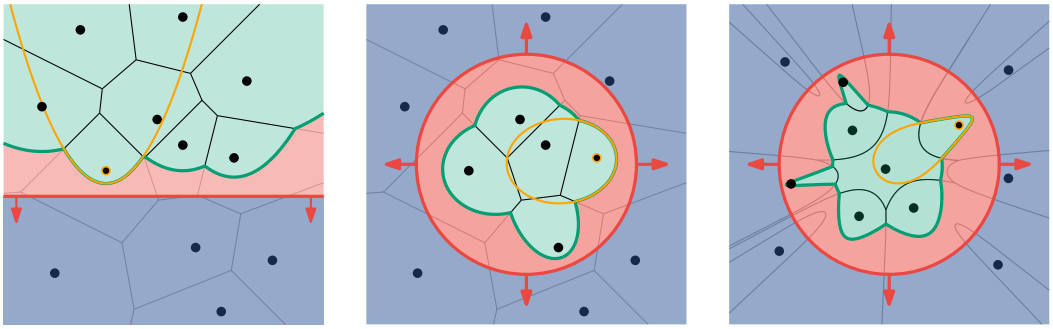
Figure 2 A point V with three sites S_1, S_2, and S_3 and the far point V' on the arc of its witness circle $\odot V$. The perpendicular bisectors of the sites intersect at V.

2.1 Hyperbolic Voronoi Diagram

The hyperbolic Voronoi diagram is defined analogously to the Euclidean version [11, Chapter 7]. Let $\mathcal{S}$ be a set of finitely many points in $\mathbb{H}^2$. For each *site* $S \in \mathcal{S}$ we define the *Voronoi cell* $\mathrm{Vor}(S)$ as the set of points $P \in \mathbb{H}^2$ such that no site in $\mathcal{S}$ is closer to P than S. The *Voronoi diagram* $\mathrm{Vor}(\mathcal{S})$ is the partition of $\mathbb{H}^2$ into the Voronoi cells. The diagram is formalized by the set $\mathcal{E}$ of *Voronoi edges* denoting the borders between cells, together with the set $\mathcal{V}$ of *Voronoi vertices* denoting the endpoints of the edges. Note that, by definition, the Voronoi edge between two sites $S_1 \neq S_2$ is a subset of the bisector $S_1 \perp S_2$. Further note that $\mathcal{V}$ contains all points $V \in \mathbb{H}^2$ that have three closest sites, i.e., $V \in \mathcal{V}$ if and only if it is the center of an empty circle $\odot V$ with at least three sites $S_1, S_2, S_3, \ldots \in \mathcal{S}$ on its arc [6]. See Figure 2 for an illustration. We call this circle the *witness circle of* V. In the context of hyperbolic Voronoi diagrams, we are often interested in the point $V' \in \odot V$, denoted as the *far point of* V, that is farthest from the pole, i.e., the point with the largest radial coordinate among points on the witness circle of V. We call the sites $S_1, S_2, S_3, \ldots$ the *incident sites* of V and refer to the tuple containing the incident sites in the order one encounters them when traversing $\odot V$ in clockwise direction starting at the far point V', as the *incidence tuple of* V.

2.2 Fortune's Algorithm

Euclidean Sweep Line. Given a set $\mathcal{S}$ of sites in the Euclidean plane, Fortune's algorithm [13] computes the Voronoi diagram $\mathrm{Vor}(\mathcal{S})$ using a *sweep line* that can be thought of as being parallel to the x-axis and traversing the plane in negative y-direction (Figure 3 (left)). At any time all sites above the sweep line are incorporated into the diagram. The sites below the sweep line have not been seen, yet, and may affect the existing diagram, at least within a certain region above the sweep line. The boundary that separates this region from the completed part of the diagram is called the *beach line*. It consists of parts of *beach parabolas*, which contain the points that lie at equal distance between a site and the sweep line. The intersections of neighboring beach parabolas trace the edges of the Voronoi diagram. Maintaining the beach line is the crucial part of the algorithm. Of course, one cannot perform a continuous sweep motion in a computer program. Instead the algorithm makes use of the fact that the beach line only changes at certain sweep line positions, called *site events* and *circle events*. Site events occur when the sweep line reaches a site and a new beach parabola is added to the beach line. A circle event occurs when the sweep line reaches the lowest point



Euclidean Sweep Line | Euclidean Sweep Circle | Hyperbolic Sweep Circle

Figure 3 Illustration of Fortune's algorithm and its adaptations. Black dots denote the sites. The sweep line (or circle) is dark red; arrows indicate its movement. The green region denotes the completed part of the diagram (black edges). The orange curve is the beach parabola (or ellipse) of the site with orange border. The beach line (or curve) is dark green. The red region denotes the part between sweep line (or circle) and beach line (or curve). Blue areas denote the unseen region.

of a circle containing three sites whose beach parabolas are consecutive on the beach line. There a parabola is potentially removed from the beach line and a Voronoi vertex is detected. For a more detailed description, we refer the reader to [11, Section 7.2].

Euclidean Sweep Circle. It was later shown that Fortune's algorithm is actually a degenerate form of a *sweep circle* algorithm [35, Theorem 1]. Instead of a sweep line that traverses the plane, the idea is to use a *sweep circle* that grows from a certain point (see Figure 3 (center)). Then, beach parabolas become *beach ellipses* that contain the points at equal distance between a site and the sweep circle, and the beach line becomes a *beach curve* consisting of beach ellipse segments. If one imagined the center of the sweep circle to lie at infinite distance to the sites, one obtains the original sweep line algorithm.

3 A Hyperbolic Sweep Circle Approach

In the polar-coordinate model, "straight" lines are hyperbolas that are bent towards the pole. Consequently, sweeping a line through the hyperbolic plane is rather tedious, as even the scheduling of site events leads to difficult computations. A much more natural approach is obtained by considering a sweep circle of expanding radius centered at the pole. This presents the first difference to the Euclidean approach: While the choice for the center of the sweep circle is basically irrelevant in Euclidean space, the pole is the only reasonable choice in the hyperbolic plane, as the occurrence of site events can be easily read from the radii of the sites then. Scheduling circle events and handling events is more involved. As shown in Figure 3 (right), the hyperbolic counterparts of beach ellipses and the beach curve are rather different from their Euclidean versions. Nevertheless, the hyperbolic sweep circle approach works analogously to the Euclidean variant. The idea is to simulate the expansion of the sweep circle, whose increasing radius we denote with $\hat{r}$, and to maintain two data structures, which we describe in the following.

3.1 Beach Curve

In the Euclidean sweep line approach the beach line consists of parts of beach parabolas. For each site $S \in \mathcal{S}$ above the sweep line, the beach parabola represents all points with equal

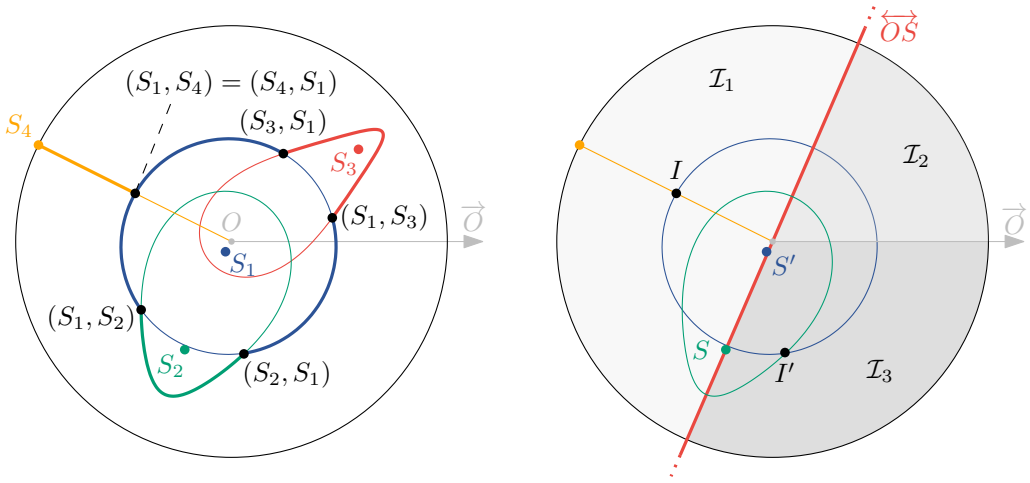


Figure 4 (Left) Four sites with beach ellipses. Since S_4 (orange) lies on the sweep circle (black), its beach ellipse is degenerate. Active segments are bold. Intersections are black points. **(Right)** We implicitly compare $\varphi(I)$ and $\varphi(I')$ using the gray sectors $\mathcal{I}_1, \mathcal{I}_2$, and $\mathcal{I}_3$ that are defined using $\overleftrightarrow{OS}$.

distance to S and the sweep line. In the Euclidean sweep circle method, the parabolas become ellipses. They are defined for sites in the sweep circle, denoted by $\mathcal{S}_{\leq \hat{r}} = \{S \in \mathcal{S} \mid r(S) \leq \hat{r}\}$, and consist of all points at equal distance to a site and the sweep circle.

In the hyperbolic plane the beach ellipse of S, denoted by $\mathcal{O}S$, is not actually elliptic (Figure 3 (right)). However, we can parameterize $\mathcal{O}S$ by the angles of the points that lie on it. To this end, we define a function $r_{\mathcal{O}S}(\varphi)$ that maps an angle $\varphi \in [0, 2\pi)$ to the radius of the point $P \in \mathcal{O}S$ with $\varphi(P) = \varphi$.

▶ **Lemma 3.** *Let $\hat{r} > 0$ be the radius of the sweep circle, let $S \in \mathcal{S}_{\leq \hat{r}}$ be a site with $r(S) < \hat{r}$, and let $P \in \mathbb{H}^2$ be a point with $\varphi(P) = \varphi$. Then, $P \in \mathcal{O}S$ if and only if P has radius*

$$r_{\mathcal{O}S}(\varphi) = \operatorname{atanh}\left(\frac{\cosh(\hat{r}) - \cosh(r(S))}{\sinh(\hat{r}) - \sinh(r(S))\cos(\varphi - \varphi(S))}\right).$$

When the site S is not inside the sweep circle, but on its arc (i.e., $r(S) = \hat{r}$), then its ellipse degenerates into the line segment $\mathcal{O}S = \overline{OS}$. The beach curve $\mathcal{B}$ is defined as the set of points lying on the outer most parts of the beach ellipses, as shown in Figure 4 (left). Formally, we define the *active segments* of a site $S \in \mathcal{S}_{\leq \hat{r}}$ as $\mathcal{A}(\mathcal{O}S) = \{P \in \mathcal{O}S \mid \nexists S' \in \mathcal{S}_{\leq \hat{r}}, P' \in \mathcal{O}S' \colon \varphi(P) = \varphi(P') \wedge r(P) < r(P')\}$. For an angular coordinate $\varphi \in [0, 2\pi)$, we say that a site S is *active at* φ, if there exists a point $P \in \mathcal{A}(\mathcal{O}S)$ with $\varphi(P) = \varphi$. The beach curve $\mathcal{B}$ is then given by the union of the active segments of sites in the sweep circle, i.e., $\mathcal{B} = \bigcup_{S \in \mathcal{S}_{\leq \hat{r}}} \mathcal{A}(\mathcal{O}S)$.

Now consider two sites $S, T \in \mathcal{S}_{\leq \hat{r}}$ together with a point P lying on an intersection of their beach ellipses. The distance between P and the sweep circle is given by $\hat{r} - r(P)$ and is, by definition of the beach ellipse, equal to $|\overline{PS}|$ and to $|\overline{PT}|$. We obtain the following.

▶ **Observation 4.** *Let $S, T \in \mathcal{S}_{\leq \hat{r}}$ be two sites with beach ellipses $\mathcal{O}S$, $\mathcal{O}T$, and let $P \in \mathcal{O}S \cap \mathcal{O}T$ be a point on an intersection of them. Then, P lies on the perpendicular bisector $S \perp T$.*

Thus, intersections of active beach ellipse segments move along the bisectors of the sites as the sweep circle expands, and trace the Voronoi edges, which are subsets of these bisectors.

We represent the beach curve $\mathcal{B}$ as a tuple $\mathcal{I}$ of intersections of active segments that are ordered by their angular coordinates. Since the beach curve is a closed curve, start and end of

the tuple are identified. Note that the angular coordinates of the intersections are constantly changing as the sweep circle expands. Therefore, we represent the intersections implicitly as a tuple of the two intersecting sites. More precisely, consider an active segment of a site S, that is bounded by the intersections I and I' with two other active segments belonging to the sites T and T', respectively. If I and I' appear in this order when traversing the beach curve in counterclockwise direction, then the segment is represented by the corresponding tuples (T, S) and (S, T') in this order. See Figure 4 (left) for an illustration of intersection tuples.

As the sweep circle expands, intersections enter and leave the beach curve $\mathcal{B}$, so $\mathcal{I}$ needs to be maintained accordingly, without knowing the angular coordinates of the intersections. For efficient insertions and deletions, we perform a binary search, while potentially reducing the number of intersections whose actual coordinates need to be computed.

Consider a new intersection I that enters the beach curve and assume that its angular coordinate $\varphi(I)$ is given. In order to find its position in the data structure $\mathcal{I}$ we want to perform a binary search and thus need to be able to decide whether $\varphi(I) < \varphi(I')$ for a given intersection $I' \in \mathcal{I}$, where $\varphi(I')$ is not known. Let $S, S' \in \mathcal{S}_{\leq \hat{r}}$ be the two sites with $I' \in \partial S \cap \partial S'$ and assume without loss of generality that $r(S) \geq r(S')$. The idea now is to use the line $\overleftrightarrow{OS}$ to decide whether $\varphi(I) < \varphi(I')$. If ∂S is degenerate, then $\varphi(I') = \varphi(S)$ and the decision is straightforward. Otherwise, we split the angular interval $[0, 2\pi)$ into three parts. Interval $\mathcal{I}_1$ contains the angles of all points lying on the opposite side of $\overleftrightarrow{OS}$ as the polar axis $\overrightarrow{O}$. Intervals $\mathcal{I}_2$ and $\mathcal{I}_3$ contain the angles on the same side of $\overleftrightarrow{OS}$ as $\overrightarrow{O}$ that are smaller and larger than $\varphi(S)$, respectively. See Figure 4 (right) for an illustration of the intervals. Then, if $\varphi(I)$ and $\varphi(I')$ are in different intervals, it is easy to decide whether $\varphi(I) < \varphi(I')$. Only if they are in the same interval we need to compute the angular coordinate of I'. Thus, it may suffice to determine the intervals that $\varphi(I)$ and $\varphi(I')$ lie in, without computing $\varphi(I')$ explicitly. Since $\varphi(I)$ is given, determining its interval is trivial. Finding the one containing $\varphi(I')$ is more involved. We can compute this information once when I' enters the beach curve, since we know its angular coordinate at this moment. Then, if $I' \in \mathcal{I}_2$, this does not change as the sweep circle expands. However, if $I' \in \mathcal{I}_1$ or $I' \in \mathcal{I}_3$, it may move from one interval to another by passing angular coordinate 0 as the sweep circle expands. Then I' moves from the first position in the beach curve data structure $\mathcal{I}$ to the last or vice versa, which we call a *structure event*. Such events are scheduled or canceled every time the first or last element in $\mathcal{I}$ changes.

In conclusion, we now know how to maintain $\mathcal{I}$ and that we can use the contained intersections to trace the Voronoi edges. It remains to determine the events at which intersections enter and leave $\mathcal{I}$ and how we can use them to detect the Voronoi vertices.

3.2 Event Queue

The second data structure the algorithm maintains is a priority queue called *event queue* $\mathcal{Q}$, which stores the events at which the beach curve changes, in the order an expanding sweep circle encounters them. That is, each event is associated with a point P and its priority is $r(P)$. Analogous to the Euclidean version (see Section 2.2), there are two types of events that change the beach curve by either adding or removing active beach ellipse segments.

An active beach ellipse segment is added to the beach curve when the sweep circle expands beyond a previously unseen site, i.e., when the radius $\hat{r}$ of the sweep circle is equal to the radial coordinate of that site. (See site S_4 in Figure 4 (left) for an example). When encountering such a *site event*, the intersections of the newly added active segment with an existing active segment are added to the tuple $\mathcal{I}$ and the bisectors between the new site and the corresponding existing site are marked as part of the Voronoi diagram. Clearly, all site

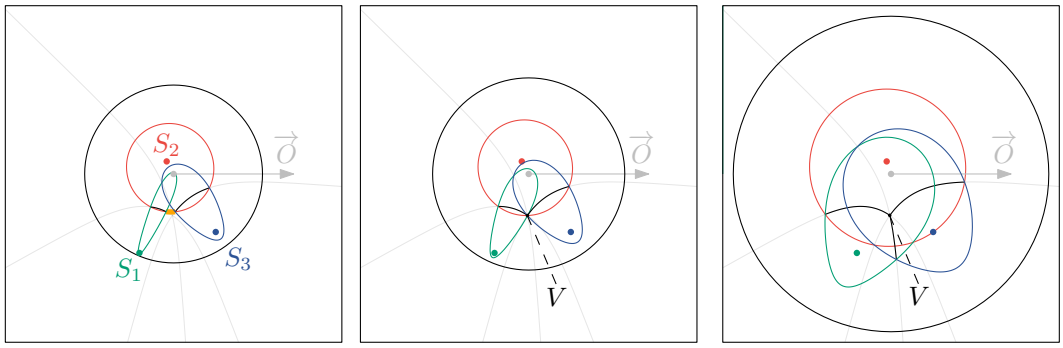


Figure 5 Beach curve intersections within an expanding sweep circle (black). **(Left)** An active segment (orange) of S_2 (red) is about to vanish. **(Center)** The active segment has vanished as the intersections of ∂S_1 and ∂S_3 with ∂S_2 meet at a point V. **(Right)** The vanished segment is replaced by a single intersection of ∂S_1 and ∂S_3.

events can be scheduled in advance, since the radial coordinates of the sites are given.

On the other hand, an active segment can be removed from the beach curve, which happens when its two intersections with other active segments merge, as shown in Figure 5. Let $S_1, S_2, S_3 \in \mathcal{S}_{\leq \hat{r}}$ be three sites such that an active segment of ∂S_2 intersects an active segment of ∂S_1 and one of ∂S_3. When the two intersections merge at a point V, then V has equal distance to the sweep circle and to the three sites S_1, S_2, and S_3. Consequently, all of them are incident to a circle $\odot V$ that is completely contained in the sweep circle. Such an event is, therefore, called *circle event*. Note that no unseen site can lie in $\odot V$. Thus, if no site is contained in $\odot V$ as the circle event occurs, then V is the center of an empty circle and, therefore, a Voronoi vertex (see Section 2.1). Then, V is added to the diagram and the bisectors of the incident sites are marked as being incident to V. Moreover, the tuple of active beach ellipse intersections $\mathcal{I}$ is adjusted, by removing the merged intersections and replacing them with a new intersection of the corresponding active segments of ∂S_1 and ∂S_3.

Such a circle event occurs when the sweep circle reaches the far point V' of V, i.e., the point with the largest radial coordinate among all points on $\odot V$. Thus, whenever an active segment enters or leaves the beach curve, we can use its intersections in $\mathcal{I}$ to determine the neighboring active segments and schedule circle events by determining the point V' for the circle the corresponding sites are incident to. We note that not all tuples of consecutive beach curve intersections lead to a circle event, as the corresponding bisectors may not intersect or the beach ellipse intersections may diverge as the sweep circle expands. Consequently, we distinguish between *true* and *false* circle events and handle them accordingly.

Instead of a continuous sweep motion, the algorithm then computes the Voronoi diagram by iteratively processing the events in the event queue, until the queue is empty.

Following the proof of correctness and the running time analysis of the Euclidean version of the algorithm (see e.g. [11, Section 7.2]) while taking our adaptations into account, we can show that the above sketched algorithm correctly computes the hyperbolic Voronoi diagram.

▶ **Theorem 5.** *Let $\mathcal{S} = \{S_1, \dots, S_n\} \subset \mathbb{H}^2$ be a set of sites. Then, the sweep circle algorithm computes* $\mathrm{Vor}(\mathcal{S})$ *in time* $\mathcal{O}(n \log(n))$.

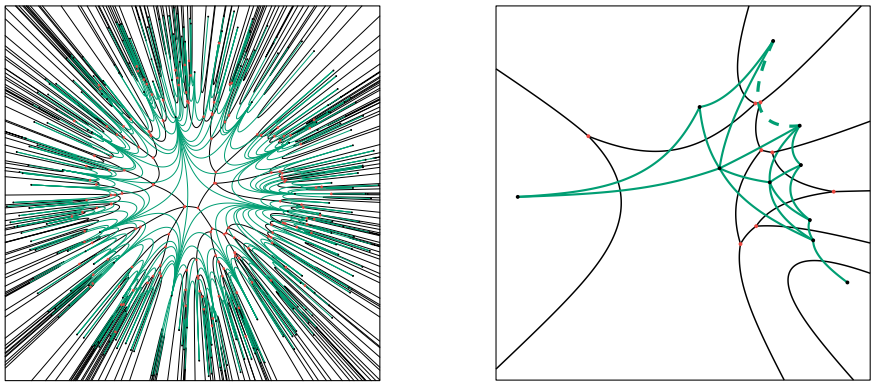


Figure 6 Voronoi diagrams for different sets of sites (black) computed using our approach, with Voronoi vertices in red and edges in black. The Delaunay complex is shown in green. **(Left)** 227 sites are distributed in a disk of radius 8.315. **(Right)** 10 sites are distributed in a disk of radius 3.171. The dashed edge was not found when using CGAL (Converted) before the fix.

4 Experiments

We implemented our algorithm[3] in C++ and compared it to the existing state-of-the-art implementation for computing two-dimensional hyperbolic Delaunay complexes in CGAL [7]. Figure 6 shows exemplary Voronoi diagrams and Delaunay complexes computed using our implementation.

Since computations in hyperbolic space are notoriously prone to numerical difficulties, the goal of the experiments is to determine how long the different approaches yield viable results as the size of the space containing the sites increases. To this end, we considered hyperbolic disks of increasing radii centered at the pole in the polar-coordinate model of the hyperbolic plane and distributed sites uniformly at random in them, according to the hyperbolic metric. Recall that the area of a hyperbolic disk of radius r grows as $2\pi(\cosh(r) - 1)$. By setting the number of sites in a disk of radius r to $N(r) = 2\pi(\cosh(c \cdot r) - 1)$ for a constant c, this number is roughly proportional to the disk area, leading to equally densely filled disks for different radii. To account for the exponential expansion of space, we then chose 10 radii in logarithmically increasing steps, up to a maximum radius of 20, and chose c such that $N(20) = 100\,000$. To obtain statistically significant results, we performed 100 samples for each disk, leading to a data set of 1000 instances. As we explain below, all experiments were, in fact, performed twice.

For each instance, we then computed the Voronoi diagram and corresponding Delaunay complex using different techniques. The first technique is the existing state-of-the-art implementation in CGAL [7], which was compiled with support enabled for the CORE library for robust numeric and geometric computation [20]. We note that this technique performs all computations in the Poincaré disk model of the hyperbolic plane (utilizing an algorithm for computing the Euclidean Voronoi diagram followed by a post-processing step in which edges not belonging to the hyperbolic diagram are removed), meaning all coordinates of the sampled sites had to be converted from the polar-coordinate model to this one, and the output of the computations (the Voronoi vertices) had to be converted back. This, of course, leads to a disadvantage as the conversions involve an exponential decrease and increase

[3] `https://github.com/maxkatzmann/fortune-hyperbolic`

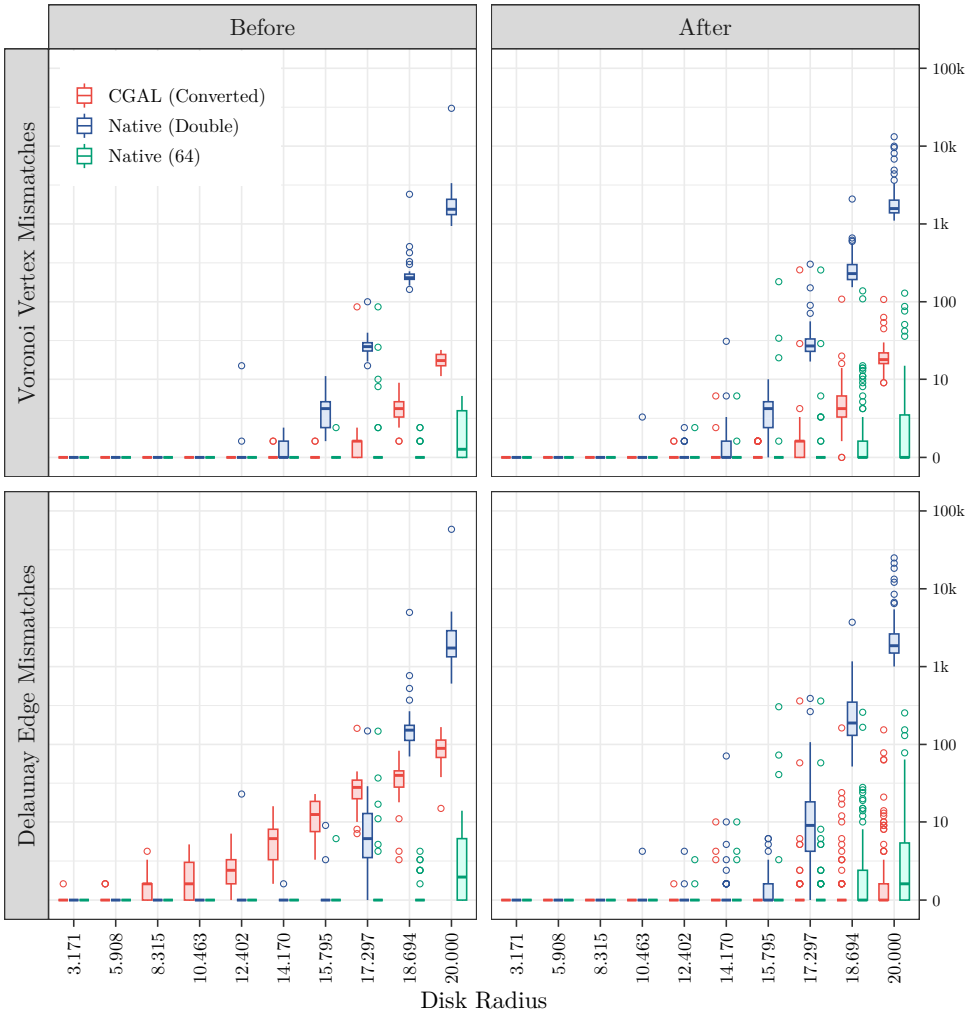


Figure 7 Comparing the robustness of different techniques for computing hyperbolic Voronoi diagrams and Delaunay complexes on sites that are distributed uniformly in disks of increasing radii. **(Top)** The number of Voronoi vertices present in the Native (128) diagram but *not* in the one obtained using the considered technique. **(Bottom)** The number of Delaunay edges present in the Native (128) complex but *not* in the one obtained by the considered the technique. **(Left)** Values obtained before we reported the issue. **(Right)** Values obtained after the issue was fixed.

of the values, respectively, which can already be affected by numerical inaccuracies. We refer to this method as *CGAL (Converted)*. Apart from that, we considered our algorithm performing all computations natively in the polar-coordinate model of the hyperbolic plane, and distinguished between different number representations. The first variant uses the *IEEE 754 Double-precision floating-point format*, which we refer to as *Native (Double)*. Additionally, we considered variants where all computations are performed using the *multiple-precision floating-point library MPFR* [14]. There, we set the precisions to 64 bits and 128 bits, and denote the corresponding techniques with *Native (64)* and *Native (128)*, respectively. We note that all values are converted to Double precision at the end, to get comparable outputs.

Unfortunately, there is no ground truth that we can compare these methods to. Instead, we consider the Native (128) variant of our algorithm as the one with the highest precision

and compared all other techniques to this one. The differences between the outputs were then quantified with respect to two measures. The first denotes for how many Voronoi vertices in the diagram computed using the Native (128) method there was no exact match in the diagram computed using the other technique, which we refer to as *Voronoi vertex mismatches*. Since comparing the structure of two diagrams is not as straight-forward, we utilize the dual of the diagram, the Delaunay complex, instead. Thus, the second measure considers the graph representing the Delaunay complex computed using the Native (128) method, and counts how many of its edges were not found in the complex computed using the other technique, which we refer to as *Delaunay edge mismatches*.

Again, since there is no ground truth, we cannot know if either implementation is correct. However, Native (128) and CGAL (Converted) produced the exact same Voronoi vertices for all 800 instances with a disk radius of at most 10.463, which we refer to as the *small disks*. Assuming that computations on larger disks were affected by numerical inaccuracies, both implementations appear to be equally correct in this regard. For the Delaunay complexes the situation is different. On all small disks CGAL (Converted) yielded the same graph *or a subgraph* of the one obtained using Native (128). However, some of the graphs computed using CGAL (Converted) were not connected (although, theoretically, the Delaunay complex always is), from which we were able to infer that this is not an issue with the Native (128) solution. As mentioned before, we reported the issue and a fix was supplied afterwards.

Figure 7 shows the box plots summarizing our experiments. There, the considered disk radii are shown on the x-axis, with the number of mismatches on the y-axis in a logarithmic scale. For each disk radius we depict three box plots (distinguished by colors) aggregating the 100 values (one for each of the instances with that radius) obtained using the different techniques. Boxes extend to the 25th and 75th percentile with the median shown as a horizontal bar, while whiskers extend to 3/2 times the interquartile range above and below the boxes. Circles denote values outside of this range.

We consider the Voronoi vertex mismatches first. As shown in Figure 7 (top row) for the small disks (of radius at most 10.463), the red boxes representing the CGAL (Converted) values degenerate into horizontal bars at 0, supporting the fact that the computed diagrams match the ones obtained using Native (128), exactly. As the disk radii increase beyond that, so does the number of considered sites in an instance and with them the Voronoi vertex mismatches. A similar trend can be seen for the other two techniques as well. Compared to CGAL (Converted) the Native (64) method shows less mismatches, while Native (Double) yielded more mismatches and did so on smaller disks, as witnessed by the outlier circles for disk radii of 10.463 and larger. We can conclude that the computation of the Voronoi vertices in the CGAL (Converted) method is more robust than the Native (Double) one, despite the conversions of the coordinates between the different models of the hyperbolic plane.

Initially, our analysis of the Delaunay edge mismatches showed a rather different behavior, see Figure 7 (bottom left). For none of the considered disk radii did CGAL (Converted) reliably match the edges obtained using Native (128). Even for the smallest considered disk radius of 3.171 there were instances where an edge was not found, as illustrated in Figure 6 (right). As with the Voronoi vertices, the edge mismatches then increase with increasing disk radii. As mentioned above, this eventually led to disconnected complexes, which is not possible in theory. For the Native (Double) method, note that the Delaunay edge mismatches align with the corresponding Voronoi vertex mismatches. That is, while the edge mismatches increase with increasing radii, we see no mismatches for the disk radii up to 8.315. The Native (64) method behaves similarly, although mismatches only start to occur at larger disk radii.

The fact that CGAL (Converted) did report the correct Voronoi vertices for smaller disk radii but not the correct Delaunay edges hinted at a possible issue in the implementation, which was reported and subsequently fixed. Consequently, we performed all experiments again with the corrected implementation. The results are shown in Figure 7 (right). As can be seen, the number of edge mismatches in CGAL (Converted) are reduced drastically and are now aligned with the corresponding Voronoi vertex mismatches. This indicates that the mismatches are a result of numerical inaccuracies.

5 Conclusion & Outlook

We present the first algorithm for computing Voronoi diagrams natively in the polar-coordinate model of the two-dimensional hyperbolic plane. We note that the distance function in this model generalizes nicely to higher dimensions, as only the computation of the angular distance between two points changes (one has to compute the central angle). Consequently, we believe that the hyperbolic sweep circle approach can be extended to higher dimensions. Furthermore, future work may consider extending the method to allow for computations of higher-order Voronoi diagrams, as they are useful in the context of nearest-neighbor queries.

Independently, the implementation of our algorithm turned out to be of interest in general as a reference that can be used to evaluate the correctness of existing implementations, highlighting that ease of implementation can be an important criterion when assessing the practicability of an algorithm. On the other hand, this emphasizes how much effort goes into maintaining fast and reliable state-of-the-art implementations, for which we are grateful.

Unfortunately, our experimental evaluation shows that neither the current state-of-the-art implementation for computing hyperbolic Voronoi diagrams and Delaunay complexes nor our solution can be used to reliably solve the problem in the polar-coordinate model of the hyperbolic plane, if the considered disk radii are sufficiently large. In particular, they are not suitable for typical applications in network science, like the aforementioned hyperbolic random graphs, where networks of 25k nodes already require disk sizes that exceed what we considered in our experiments.

Thus, since none of the considered approaches seems to be able to scale to such large areas, further extensions are necessary to make them more robust. Alternatively, it may prove worthwhile to examine adaptations of other approaches to computing Voronoi diagrams, like randomized incremental construction [19], divide and conquer [32], utilizing variants of abstract Voronoi diagrams [21], or a topology-oriented method [33].

Nevertheless, our method is the first stepping stone towards applying hyperbolic Voronoi diagrams and Delaunay complexes in the ongoing study of complex networks utilizing the polar-coordinate model of the hyperbolic plane. In the following, we briefly highlight a direct application of our algorithm in this context, which is the computation of the hyperbolic counterpart to Euclidean minimum spanning trees. To the best of our knowledge *hyperbolic random minimum spanning trees* have not been studied before, but may prove useful as the tree equivalent to the aforementioned hyperbolic random graph model [22]. Analogous to the Euclidean version, the hyperbolic minimum spanning tree is a subgraph of the Delaunay complex of a given set of sites, meaning it can be computed in time $\mathcal{O}(n \log(n))$ using our approach. Consequently, it would be interesting to utilize hyperbolic Delaunay complexes in the polar-coordinate model to generate and investigate trees in the hyperbolic plane.

References

1 Gregorio Alanis-Lobato, Pablo Mier, and Miguel Andrade-Navarro. The latent geometry of the human protein interaction network. *Bioinformatics*, 34(16):2826–2834, 2018. doi:10.1093/bioinformatics/bty206.

2 Marshall Bern and David Eppstein. Optimal Möbius Transformations for Information Visualization and Meshing. In *Algorithms and Data Structures (WADS)*, pages 14–25, 2001. doi:10.1007/3-540-44634-6_3.

3 Thomas Bläsius, Philipp Fischbeck, Tobias Friedrich, and Maximilian Katzmann. Solving vertex cover in polynomial time on hyperbolic random graphs. *Theory of Computing Systems*, 2021. doi:10.1007/s00224-021-10062-9.

4 Thomas Bläsius, Cedric Freiberger, Tobias Friedrich, Maximilian Katzmann, Felix Montenegro-Retana, and Marianne Thieffry. Efficient Shortest Paths in Scale-Free Networks with Underlying Hyperbolic Geometry. In *International Colloquium on Automata, Languages, and Programming (ICALP)*, pages 20:1–20:14, 2018. doi:10.4230/LIPIcs.ICALP.2018.20.

5 Martin Bock, Amit Kumar Tyagi, Jan-Ulrich Kreft, and Wolfgang Alt. Generalized Voronoi Tessellation as a Model of Two-dimensional Cell Tissue Dynamics. *Bulletin of Mathematical Biology*, 72(7):1696–1731, 2010. doi:10.1007/s11538-009-9498-3.

6 Mikhail Bogdanov, Olivier Devillers, and Monique Teillaud. Hyperbolic Delaunay complexes and Voronoi diagrams made practical. *Journal of Computational Geometry*, 5:56–85, 2014. doi:10.20382/JOCG.V5I1A4.

7 Mikhail Bogdanov, Iordan Iordanov, and Monique Teillaud. 2D Hyperbolic Delaunay Triangulations. In *CGAL User and Reference Manual*. CGAL Editorial Board, 5.4 edition, 2022. URL: https://doc.cgal.org/5.4/Manual/packages.html#PkgHyperbolicTriangulation2.

8 Marian Boguna, Fragkiskos Papadopoulos, and Dmitri Krioukov. Sustaining the Internet with Hyperbolic Mapping. *Nature Communications*, 1(1):62, 2010. doi:10.1038/ncomms1063.

9 Jean-Daniel Boissonnat, André Cérézo, Olivier Devillers, and Monique Teillaud. Output-sensitive construction of the Delaunay triangulation of points lying in two planes. *International Journal of Computational Geometry and Applications*, 06(01):1–14, 1996. doi:10.1142/S0218195996000022.

10 Jean-Daniel Boissonnat and Mariette Yvinec. Non-euclidean metrics. In *Algorithmic Geometry*, page 433–458. Cambridge University Press, 1998. doi:10.1017/CBO9781139172998.025.

11 Mark de Berg, Otfried Cheong, Marc van Kreveld, and Mark Overmars. *Computational Geometry: Algorithms and Applications*. Springer, 2008.

12 David S. Ebert, F. Kenton Musgrave, Darwyn Peachey, Ken Perlin, and Steven Worley. *Texturing and Modeling: A Procedural Approach*. Elsevier Science, 2002.

13 Steven Fortune. A sweepline algorithm for Voronoi diagrams. In *Symposium on Computational Geometry (SoCG)*, page 313–322, 1986. doi:10.1145/10515.10549.

14 Laurent Fousse, Guillaume Hanrot, Vincent Lefèvre, Patrick Pélissier, and Paul Zimmermann. Mpfr: A multiple-precision binary floating-point library with correct rounding. *ACM Trans. Math. Softw.*, 33(2):13–es, 2007. doi:10.1145/1236463.1236468.

15 Tobias Friedrich, Maximilian Katzmann, and Leon Schiller. Computing voronoi diagrams in the polar-coordinate model of the hyperbolic plane. *CoRR*, abs/2112.02553, 2021. URL: https://arxiv.org/abs/2112.02553.

16 Guillermo García-Pérez, Marián Boguñá, Antoine Allard, and M. Serrano. The hidden hyperbolic geometry of international trade: World trade atlas 1870–2013. *Scientific Reports*, 6:33441, 2016. doi:10.1038/srep33441.

17 Santiago Garrido, Luis Moreno, Mohamed Abderrahim, and Fernando Martin. Path Planning for Mobile Robot Navigation using Voronoi Diagram and Fast Marching. In *2006 IEEE/RSJ International Conference on Intelligent Robots and Systems*, pages 2376–2381, 2006. doi:10.1109/IROS.2006.282649.

18 Luca Gugelmann, Konstantinos Panagiotou, and Ueli Peter. Random hyperbolic graphs: Degree sequence and clustering. In *International Colloquium on Automata, Languages, and Programming (ICALP)*, page 573–585, 2012. doi:10.1007/978-3-642-31585-5_51.

19 Leonidas J. Guibas, Donald E. Knuth, and Micha Sharir. Randomized incremental construction of delaunay and voronoi diagrams. In Michael S. Paterson, editor, *Automata, Languages and Programming*, pages 414–431, Berlin, Heidelberg, 1990. Springer Berlin Heidelberg.

20 V. Karamcheti, C. Li, I. Pechtchanski, and C. Yap. A core library for robust numeric and geometric computation. In *Proceedings of the Fifteenth Annual Symposium on Computational Geometry*, page 351–359, 1999. doi:10.1145/304893.304989.

21 Rolf Klein. *Concrete and Abstract Voronoi Diagrams*. Springer, Berlin, Heidelberg, 1989. doi:10.1007/3-540-52055-4.

22 Dmitri Krioukov, Fragkiskos Papadopoulos, Maksim Kitsak, Amin Vahdat, and Marián Boguñá. Hyperbolic geometry of complex networks. *Physical Review E*, 82:036106, 2010. doi:10.1103/PhysRevE.82.036106.

23 Anton Krohmer. *Structures & algorithms in hyperbolic random graphs*. Dissertation, Universität Potsdam, 2016.

24 Richard G. Lyons. Sum of two sinusoids. 2011. URL: https://dspguru.com/files/Sum_of_Two_Sinusoids.pdf.

25 Tobias Müller and Merlijn Staps. The diameter of KPKVB random graphs. *Advances in Applied Probability*, 51(2):358–377, 2019. doi:10.1017/apr.2019.23.

26 Frank Nielsen. On Voronoi Diagrams on the Information-Geometric Cauchy Manifolds. *Entropy*, 22(7), 2020. doi:10.3390/e22070713.

27 Frank Nielsen and Richard Nock. Hyperbolic Voronoi Diagrams Made Easy. In *International Conference on Computational Science and Its Applications (ICCSA)*, page 74–80, 2010. doi:10.1109/ICCSA.2010.37.

28 Frank Nielsen and Richard Nock. Visualizing Hyperbolic Voronoi Diagrams. In *Proceedings of the Thirtieth Annual Symposium on Computational Geometry*, page 90–91, 2014. doi:10.1145/2582112.2595647.

29 Zahra Nilforoushan and Ali Mohades. Hyperbolic Voronoi Diagram. In *Computational Science and Its Applications (ICCSA)*, page 735–742, 2006. doi:10.1007/11751649_81.

30 Kensuke Onishi and Nobuki Takayama. Construction of Voronoi Diagram on the Upper Half-Plane. *IEICE Transactions on Fundamentals of Electronics, Communications and Computer Sciences*, 79:533–539, 1996.

31 Arlan Ramsay and Robert D. Richtmyer. *Introduction to Hyperbolic Geometry*. Springer, 1995. doi:10.1007/978-1-4757-5585-5.

32 Michael Ian Shamos and Dan Hoey. Closest-point problems. In *16th Annual Symposium on Foundations of Computer Science (sfcs 1975)*, pages 151–162, 1975. doi:10.1109/SFCS.1975.8.

33 Kokichi Sugihara and Masao Iri. A Robust Topology-Oriented Incremental Algorithm for Voronoi Diagrams. *International Journal of Computational Geometry & Applications*, 04(02):179–228, 1994. doi:10.1142/S0218195994000124.

34 Toshihiro Tanuma, Hiroshi Imai, and Sonoko Moriyama. *Revisiting Hyperbolic Voronoi Diagrams in Two and Higher Dimensions from Theoretical, Applied and Generalized Viewpoints*, pages 1–30. Springer Berlin Heidelberg, 2011. doi:10.1007/978-3-642-25249-5_1.

35 Shi-Qing Xin, Xiaoning Wang, Jiazhi Xia, Wolfgang Mueller-Wittig, Guo-Jin Wang, and Ying He. Parallel computing 2D Voronoi diagrams using untransformed sweepcircles. *Computer-Aided Design*, 45(2):483–493, 2013. doi:10.1016/j.cad.2012.10.031.

A Missing Proofs

In the following, we give the proofs that were left out of the main part of the paper due to space constraints.

A.1 Preliminaries

▶ **Lemma 1.** *Let $\triangle ABC$ and $\triangle ABC'$ be triangles with $|\overline{BC}| = |\overline{BC'}|$ and angles φ and φ' at B, respectively. Then, $\varphi < \varphi'$ (resp. $\varphi > \varphi'$) if and only if $|\overline{AC}| < |\overline{AC'}|$ (resp. $|\overline{AC}| > |\overline{AC'}|$).*

Proof. We prove the claim for the case where $\varphi < \varphi'$. The proof for the other case is analogous. We start by showing that changing the angle also changes the length of the line segment accordingly. Since φ, φ' are inner angles of triangles, we have $\varphi, \varphi' \in [0, \pi)$ and thus $\cos(\varphi) > \cos(\varphi')$. We can now determine $|\overline{AC}|$ using the hyperbolic law of cosines and make use of the fact that $|\overline{BC}| = |\overline{BC'}|$, which yields

$$\begin{aligned}
|\overline{AC}| &= \operatorname{acosh}\left(\cosh(|\overline{AB}|)\cosh(|\overline{BC}|) - \sinh(|\overline{AB}|)\sinh(|\overline{BC}|)\cos(\varphi)\right) \\
&= \operatorname{acosh}\left(\cosh(|\overline{AB}|)\cosh(|\overline{BC'}|) - \sinh(|\overline{AB}|)\sinh(|\overline{BC'}|)\cos(\varphi)\right) \\
&< \operatorname{acosh}\left(\cosh(|\overline{AB}|)\cosh(|\overline{BC'}|) - \sinh(|\overline{AB}|)\sinh(|\overline{BC'}|)\cos(\varphi')\right) \\
&= |\overline{AC'}|,
\end{aligned}$$

where the inequality is due to the fact that $\cos(\varphi) > \cos(\varphi')$ and that $\operatorname{acosh}(x)$ is strictly increasing with increasing x.

It remains to prove that changing the length of the line segment also changes the angle accordingly. Note that $|\overline{AC}| < |\overline{AC'}|$ implies $\cosh(|\overline{AC}|) < \cosh(|\overline{AC'}|)$, since $\cosh(x)$ is strictly increasing for increasing $x \geq 0$. Again, using the hyperbolic law of cosines, we can express φ using the lengths of the line segments in $\triangle ABC$ as

$$\begin{aligned}
\varphi &= \operatorname{acos}\left(\frac{\cosh(|\overline{AB}|)\cosh(|\overline{BC}|) - \cosh|\overline{AC}|}{\sinh(|\overline{AB}|)\sinh(|\overline{BC}|)}\right) \\
&= \operatorname{acos}\left(\frac{\cosh(|\overline{AB}|)\cosh(|\overline{BC'}|) - \cosh|\overline{AC}|}{\sinh(|\overline{AB}|)\sinh(|\overline{BC'}|)}\right) \\
&< \operatorname{acos}\left(\frac{\cosh(|\overline{AB}|)\cosh(|\overline{BC'}|) - \cosh|\overline{AC'}|}{\sinh(|\overline{AB}|)\sinh(|\overline{BC'}|)}\right) \\
&= \varphi',
\end{aligned}$$

where the inequality is due to the fact that $\cosh(|\overline{AC}|) < \cosh(|\overline{AC'}|)$ and that $\operatorname{acos}(x)$ is strictly decreasing for increasing x. ◀

▶ **Lemma 2.** *Let $\triangle ABC$ be a triangle with $|\overline{AB}| \leq |\overline{AC}|$. For every $d \in [|\overline{AB}|, |\overline{AC}|]$, there exists a point $P \in \overline{BC}$ with $|\overline{AP}| = d$.*

Proof. For $d = |\overline{AB}|$ or $d = |\overline{AC}|$, the points $P = B$ and $P = C$ fulfill the requirements of the lemma, respectively. So assume that $d \in (|\overline{AB}|, |\overline{AC}|)$. Now consider the circle $\odot A$ of radius d around A. Since $|\overline{AB}| < d$, the point B is inside the circle. Moreover, since $|\overline{AC}| > d$, the point C is outside the circle. Consequently, the line segment $\overline{BC}$ intersects the circle at a point $P = \overline{BC} \cap \odot A$. In particular, $P \in \odot A$ and thus $|\overline{AP}| = d$. ◀

A.2 Beach Curve

▶ **Lemma 3.** *Let $\hat{r} > 0$ be the radius of the sweep circle, let $S \in \mathcal{S}_{\leq \hat{r}}$ be a site with $r(S) < \hat{r}$, and let $P \in \mathbb{H}^2$ be a point with $\varphi(P) = \varphi$. Then, $P \in \partial S$ if and only if P has radius*

$$r_{\partial S}(\varphi) = \operatorname{atanh}\left(\frac{\cosh(\hat{r}) - \cosh(r(S))}{\sinh(\hat{r}) - \sinh(r(S))\cos(\varphi - \varphi(S))}\right).$$

Proof. By definition, we have $P \in \partial S$ if and only if P is equidistant to S and the sweep circle. Since the distance between a point and a circle centered at the origin is given by the difference of their radii, P needs to fulfill the equality

$$|\overline{PS}| = \hat{r} - r(P).$$

Applying Equation 2, which describes the hyperbolic distance between two points, together with an application of the hyperbolic cosine on both sides then yields

$$\cosh(r(P))\cosh(r(S)) - \sinh(r(P))\sinh(r(S))\cos(\varphi(P) - \varphi(S)) = \cosh(\hat{r} - r(P)).$$

We can now apply the identity $\cosh(x - y) = \cosh(x)\cosh(y) - \sinh(x)\sinh(y)$ to the right hand side and obtain

$$\cosh(r(P))\cosh(r(S)) - \sinh(r(P))\sinh(r(S))\cos(\varphi(P) - \varphi(S)) = \cosh(\hat{r})\cosh(r(P)) - \sinh(\hat{r})\sinh(r(P)).$$

We continue by subtracting $\cosh(\hat{r})\cosh(r(P))$ on both sides and adding $\sinh(\hat{r})\sinh(r(P))$, which yields

$$\sinh(\hat{r})\sinh(r(P)) - \sinh(r(P))\sinh(r(S))\cos(\varphi(P) - \varphi(S)) = \cosh(\hat{r})\cosh(r(P)) - \cosh(r(P))\cosh(r(S)).$$

By factoring out $\sinh(r(P))$ and $\cosh(r(P))$, we get

$$\sinh(r(P))\big(\sinh(\hat{r}) - \sinh(r(S))\cos(\varphi(P) - \varphi(S))\big) = \cosh(r(P))\big(\cosh(\hat{r}) - \cosh(r(S))\big),$$

which is equivalent to

$$\frac{\sinh(r(P))}{\cosh(r(P))} = \frac{\cosh(\hat{r}) - \cosh(r(S))}{\sinh(\hat{r}) - \sinh(r(S))\cos(\varphi(P) - \varphi(S))},$$

after dividing by $\cosh(r(P))$ and $\sinh(\hat{r}) - \sinh(r(S))\cos(\Delta_\varphi(P, S))$ on both sides. Finally, we recognize that the left hand side is the hyperbolic tangent $\tanh(r(P))$. Applying the inverse hyperbolic tangent then yields the claim. ◀

A.3 Correctness and Complexity

In this section, we present the components for the proof of our main theorem.

▶ **Theorem 5.** *Let $\mathcal{S} = \{S_1, \dots, S_n\} \subset \mathbb{H}^2$ be a set of sites. Then, the sweep circle algorithm computes* $\mathrm{Vor}(\mathcal{S})$ *in time $\mathcal{O}(n \log(n))$.*

Like the algorithm itself, the proof of its correctness works analogous to the Euclidean version [11, Section 7.2]. Therefore, we only focus on the main parts of the proof and show that they also hold for the hyperbolic sweep circle approach. In particular, we show that the only way in which a new beach ellipse segment can appear on the beach curve is through a site event (Lemma 15), the only way in which an existing segment can disappear from the beach curve is through a circle event (Lemma 17), and that every Voronoi vertex is detected by means of a circle event (Lemma 18).

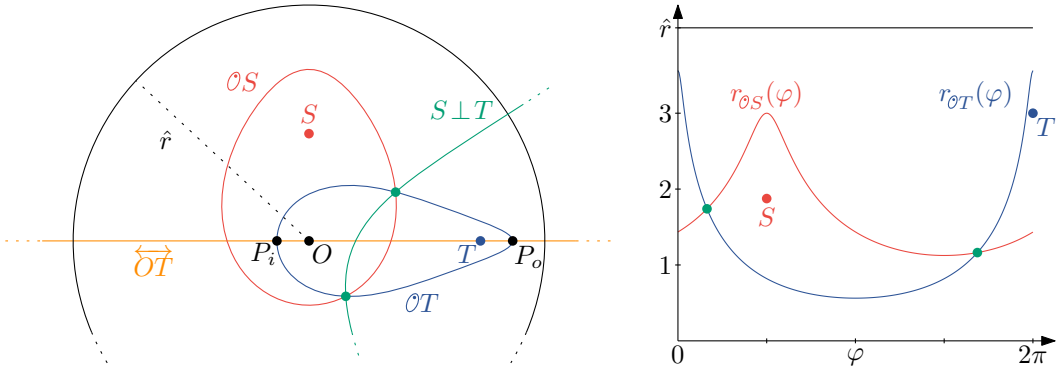


Figure 8 (Left) Two sites S, T inside the sweep circle (black). The points P_i and P_o are on ∂T (blue) and are inside and outside of ∂S (red), respectively. The intersections (green points) of the ellipses are on the perpendicular bisector $S \perp T$ (green) and on opposite sites of the line $\overleftrightarrow{OT}$ (orange). **(Right)** The functions $r_{\partial S}(\varphi)$ and $r_{\partial T}(\varphi)$ describe the arcs of the beach ellipses on the left.

A.3.1 Beach Ellipse Intersections

To start, we establish some basic properties of beach ellipse intersections in the hyperbolic plane, beginning with their existence. Given a site $S \in \mathcal{S}_{\leq \hat{r}}$, we say that a point P is *inside* the beach ellipses ∂S, if $|\overline{PS}|$ is smaller than the distance between P and the sweep circle. If $|\overline{PS}|$ is larger instead, we say that P is *outside* of ∂S. The following lemma shows that, given two distinct sites inside the sweep circle, the beach ellipse of one contains two points that are inside and outside of the ellipse of the other, respectively, as illustrated in Figure 8 (left).

▶ **Lemma 6.** *Let $\hat{r}$ be the radius of the sweep circle, let $S \neq T \in \mathcal{S}_{\leq \hat{r}}$ be two sites with $0 < r(S) \leq r(T) < \hat{r}$ and let ∂S and ∂T be their beach ellipses. Then the point $P_i \in \partial T$ with $\varphi(P_i) = \varphi(T) + \pi$ is inside of ∂S and $P_o \in \partial T$ with $\varphi(P_o) = \varphi(T)$ is outside of ∂S.*

Proof. Assume, without loss of generality, that $\varphi(T) = 0$. To show that P_i is inside of ∂S, we show that the distance between P_i and the sweep circle is larger than $|\overline{P_iS}|$. More precisely, since $P_i \in \partial T$, P_i is equidistant to the sweep circle and to T. Consequently, it suffices to show that $|\overline{P_iT}| > |\overline{P_iS}|$. We now distinguish several cases depending on the position of S. If $\varphi(S) = \varphi(T)$, then we have $r(S) < r(T)$ (since $S \neq T$) and thus

$$|\overline{P_iT}| = r(P_i) + r(T) > r(P_i) + r(S) = |\overline{P_iS}|.$$

If $\varphi(S) = \varphi(T) + \pi$, we first consider the case where $r(S) \geq r(P_i)$. Then,

$$|\overline{P_iT}| = r(P_i) + r(T) \geq r(P_i) + r(S) > r(S) - r(P_i) = |\overline{P_iS}|.$$

Alternatively, if $\varphi(S) = \varphi(T) + \pi$ and $r(S) < r(P_i)$, we have

$$|\overline{P_iT}| = |\overline{P_iS}| + r(S) + r(T) > |\overline{P_iS}|.$$

In all other cases, we can consider the triangle $\triangle OSP_i$. Since the area of this triangle is non-zero, we can apply the strict triangle inequality, which yields $|\overline{P_iS}| < r(P_i) + r(S)$. It follows that

$$|\overline{P_iT}| = r(P_i) + r(T) \geq r(P_i) + r(S) > |\overline{P_iS}|.$$

Consequently, in all cases P_i is closer to S than to the sweep circle, and is therefore inside ∂S. Proving that P_o is outside of ∂S works analogously. We show that P_o is closer to the sweep

circle than to S, which is equivalent to showing $|\overline{P_oT}| < |\overline{P_oS}|$, since P_o is equidistant to T and the sweep circle. We again distinguish several cases depending on the position of S. If $\varphi(S) = \varphi(T)$, the distinctness of S and T implies $r(S) < r(T)$ and thus

$$|\overline{P_oT}| = r(P_o) - r(T) < r(P_o) - r(S) = |\overline{P_oS}|.$$

Similarly, if $\varphi(S) = \varphi(T) + \pi$, we have

$$|\overline{P_oT}| = r(P_o) - r(T) < r(P_o) + r(S) = |\overline{P_oS}|.$$

Again, in all other cases, we can apply the strict triangle inequality to conclude $r(P_o) < r(S) + |\overline{P_oS}|$ or equivalently $r(P_o) - r(S) < |\overline{P_oS}|$. Thus,

$$|\overline{P_oT}| = r(P_o) - r(T) \leq r(P_o) - r(S) < |\overline{P_oS}|,$$

which shows that P_o is outside of $\mathcal{O}S$ in all cases. ◀

With the above lemma we can now prove that two non-degenerate beach ellipses intersect in exactly two points. If one of them is degenerate, they intersect in exactly one point.

▶ **Lemma 7.** *Let $\hat{r}$ be the radius of the sweep circle, let $S \neq T \in \mathcal{S}_{\leq \hat{r}}$ be two sites with $0 < r(S) \leq r(T)$ and let $\mathcal{O}S$ and $\mathcal{O}T$ be their beach ellipses. Then, $\mathcal{O}S \cap \mathcal{O}T$ contains two points if $r(S), r(T) < \hat{r}$ and one point, otherwise.*

Proof. We start with the non-degenerate case and show that the number of intersections is at least two and that it is at most two. By Lemma 3, the beach ellipse of S is described by a function $r_{\mathcal{O}S}(\varphi)$ that maps an angle φ to the radius of the point $P \in \mathcal{O}S$ with $\varphi(P) = \varphi$, see Figure 8 (right). Analogously, there is a function $r_{\mathcal{O}T}(\varphi)$ for $\mathcal{O}T$. As shown in Lemma 6, there are two points $P_i, P_o \in \mathcal{O}T$ that are inside and outside of $\mathcal{O}S$, respectively. Thus, $r_{\mathcal{O}S}(\varphi(P_i)) > r_{\mathcal{O}T}(\varphi(P_i))$ and $r_{\mathcal{O}S}(\varphi(P_o)) < r_{\mathcal{O}T}(\varphi(P_o))$. Since $r_{\mathcal{O}S}(\varphi), r_{\mathcal{O}T}(\varphi)$ are continuous and periodic functions with a period of 2π (see Lemma 3), we can apply the intermediate value theorem to conclude that there are at least two values $\varphi \in [0, 2\pi)$ such that $r_{\mathcal{O}S}(\varphi) = r_{\mathcal{O}T}(\varphi)$.

We now show that there are at most two intersections. The angular coordinates of all intersections are obtained by solving $r_{\mathcal{O}S}(\varphi) = r_{\mathcal{O}T}(\varphi)$ for φ. By Lemma 3, this happens when

$$\frac{\cosh(\hat{r}) - \cosh(r(S))}{\sinh(\hat{r}) - \sinh(r(S))\cos(\varphi - \varphi(S))} = \frac{\cosh(\hat{r}) - \cosh(r(T))}{\sinh(\hat{r}) - \sinh(r(T))\cos(\varphi - \varphi(T))}.$$

Note that solving this equation for φ is equivalent to finding the roots of the function $f(\varphi) = a\cos(\varphi - \varphi(S)) - b\cos(\varphi - \varphi(T)) + c$, where the constants a, b, and c are defined as

$$a = (\cosh(\hat{r}) - \cosh(r(T)))\sinh(r(S)), \text{ and } b = (\cosh(\hat{r}) - \cosh(r(S)))\sinh(r(T)), \text{ and}$$
$$c = (\cosh(r(T)) - \cosh(r(S)))\sinh(\hat{r}).$$

Note that $f(\varphi)$ is the sum of two differently phased cosine functions of equal frequency with amplitudes a and b, respectively, together with a constant c. Since the sum of two sinusoids of the same frequency is another sinusoid, we can use [24, Equation (6)], to conclude that $f(\varphi) = a'\cos(\varphi + \xi) + c$, where the constants a' and ξ are given by

$$a' = \sqrt{(a\cos(\varphi(S)) + b\cos(\varphi(T)))^2 + (a\sin(\varphi(S)) + b\sin(\varphi(T)))^2},$$
$$\xi = \operatorname{atan}\left(\frac{a\sin(\varphi(S)) + b\sin(\varphi(T))}{a\cos(\varphi(S)) + b\cos(\varphi(T))}\right),$$

and a, b, and c are defined as above. Consequently, $f(\varphi)$ is a cosine function with amplitude a' and period 2π, which has at most two roots in $[0, 2\pi)$ if $a' \neq 0$. Therefore, it remains to show that a' is non-zero. First note that a' only vanishes if both sums in the quadratic functions do. Since there exists no $x \in \mathbb{R}$ such that $\cos(x) = 0$ *and* $\sin(x) = 0$, it follows that a' is non-zero as long as a and b are non-zero. Since $\mathcal{O}S$ and $\mathcal{O}T$ are non-degenerate, we know that $r(S), r(T) < \hat{r}$, and since $\cosh(x)$ is strictly increasing for $x \geq 0$, we have

$$\cosh(\hat{r}) - \cosh(r(S)) > 0 \text{ and } \cosh(\hat{r}) - \cosh(r(T)) > 0.$$

Moreover, since $r(S), r(T) > 0$ by assumption, it follows that $\sinh(r(S)), \sinh(r(T)) > 0$, which concludes the proof of the non-degenerate case.

If $\mathcal{O}S$ is degenerate, then $\mathcal{O}S = \overline{OS}$ and all intersections in $\mathcal{O}S \cap \mathcal{O}T$ have angular coordinate $\varphi(S)$. Thus, by Lemma 3, there is only one point $P \in \mathcal{O}T$ satisfying $\varphi(P) = \varphi(S)$. Analogously, there is only one intersection when $\mathcal{O}T$ is degenerate but $\mathcal{O}S$ is not. Finally, when both sites are degenerate, i.e., $r(S) = r(T) = \hat{r}$, then $\varphi(S) \neq \varphi(T)$, since both sites are assumed to be distinct. In that case, the two ellipses $\mathcal{O}S = \overline{OS}$ and $\mathcal{O}T = \overline{OT}$ intersect only in the pole. ◀

We continue by investigating how the intersections move as the sweep circle expands. To this end, we first show that the beach ellipses expand as well.

▶ **Lemma 8.** *Let $S \in \mathcal{S}_{\leq \hat{r}}$ be a site and let r_1, r_2 be two radii with $r(S) \leq r_1 < r_2$. Then, $\mathcal{O}S$ at $\hat{r} = r_1$ is inside of $\mathcal{O}S$ at $\hat{r} = r_2$.*

Proof. Consider a point $P \in \mathcal{O}S$ as $\hat{r} = r_1$. Then, the distance between P and the sweep circle is given by $r_1 - r(P)$ and is equal to $|\overline{PS}|$. At $\hat{r} = r_2$, $|\overline{PS}|$ remains unchanged. However, then the distance between P and the sweep circle increases to $r_2 - r(P) > r_1 - r(P) = |\overline{PS}|$. It follows that P is closer to S than to the sweep circle at $\hat{r} = r_2$ and is therefore inside $\mathcal{O}S$. ◀

We are now ready to show that the two beach ellipse intersections of a pair of sites S and T start at the same point and move along the bisector $S \perp T$ in opposite directions as the radius $\hat{r}$ of the sweep circle increases.

▶ **Lemma 9.** *Let $S \neq T \in \mathcal{S}_{\leq \hat{r}}$ be two sites with $r(S) \leq r(T)$ and consider the intersections $I, I' \in \mathcal{O}S \cap \mathcal{O}T$ and the point $P = \overline{OT} \cap S \perp T$. For $\hat{r} = r(T)$, we have $I = I' = P$. For $\hat{r} > r(T)$, I and I' are on opposite sides of $\overleftrightarrow{OT}$. As $\hat{r}$ increases, so do $|\overline{PI}|$ and $|\overline{PI'}|$.*

Proof. For $\hat{r} = r(T)$, the beach ellipse $\mathcal{O}T$ is degenerate and consists of the line segment $\overline{OT}$. By Lemma 7, the two ellipses $\mathcal{O}S$ and $\mathcal{O}T$ intersect in a single point. This point is P as the intersection is on $\mathcal{O}T = \overline{OT}$ and has by definition equal distance to S and T, i.e., it lies on $S \perp T$. Moreover, this point is unique, as $\overline{OT} \not\subset S \perp T$, since $T \in \overline{OT}$ but $T \notin S \perp T$.

We continue with the proof that I and I' are on opposite sides of $\overleftrightarrow{OT}$ for $\hat{r} > r(T)$, as shown in Figure 8 (left). Without loss of generality, assume that $\varphi(T) = 0$ and consider the points $P_i, P_o \in \mathcal{O}T$ as defined in Lemma 6, that are inside and outside of $\mathcal{O}S$, respectively. That is, $r_{\mathcal{O}T}(0) > r_{\mathcal{O}S}(0)$ and $r_{\mathcal{O}T}(\pi) < r_{\mathcal{O}S}(\pi)$. Consequently, one of I and I' has an angular coordinate in $(0, \pi)$ and the other in $(\pi, 2\pi)$. Thus, they are on opposite sides of $\overleftrightarrow{OT}$.

It remains to show that $|\overline{PI}|$ and $|\overline{PI'}|$ increase with $\hat{r}$. Consider two radii r_1, r_2 with $r(T) \leq r_1 < r_2$. Let I_{r_1} and I_{r_2} denote the positions that the intersection I has at $\hat{r} = r_1$ and $\hat{r} = r_2$, respectively, and let I'_{r_1} and I'_{r_2} be defined analogously. Consider $\hat{r} = r_1$ first. By Lemma 7 the bisector $S \perp T$ intersects $\mathcal{O}T$ at exactly the points I_{r_1} and I'_{r_1}, meaning the line segment $\overline{I_{r_1} I'_{r_1}}$ lies in $\mathcal{O}T$. Moreover, the point P lies in $\mathcal{O}T$ and on $S \perp T$, meaning $P \in \overline{I_{r_1} I'_{r_1}}$

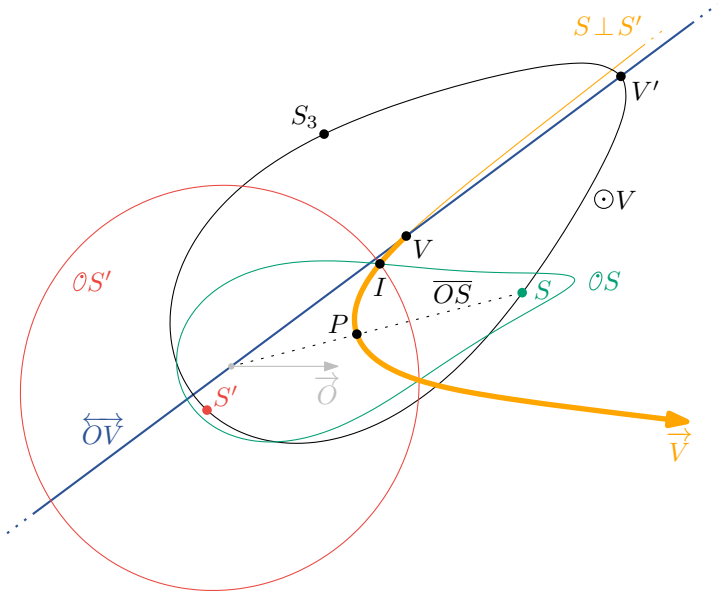


Figure 9 Illustration of the proof of Lemma 10. The sites S and S' lie on the witness circle of V. The intersection $I \in \partial S \cap \partial S'$ that moves towards V lies on the angular bisector $\overrightarrow{V}$ (orange) of the angle $\sphericalangle SVS'$, since $\overrightarrow{V}$, I, P, and S are on the same side of $\overleftrightarrow{OV}$.

and thus the line segments $\overline{PI_{r_1}}$ and $\overline{PI'_{r_1}}$ are contained in ∂T. Now assume that $\hat{r}$ increases to $\hat{r} = r_2$ but $|\overline{PI}|$ does not. (The proof for $|\overline{PI'}|$ is analogous.) Then $I_{r_2} \in \overline{PI_{r_1}}$. However, since the beach ellipse ∂T at $\hat{r} = r_1$ is completely contained in ∂T at $\hat{r} = r_2$ (Lemma 8), it follows that $I_{r_2} \in \overline{PI_{r_1}}$ is inside of ∂T, contradicting the fact that $I_{r_2} \in \partial T$. ◀

The above lemma has some interesting implications. Consider two sites S, T that are incident to a Voronoi vertex V, meaning they lie on the arc of the witness circle of V. Then, V lies on the bisector $S \perp T$ and, in particular, on one side of the point $P \in S \perp T$ defined in the lemma. As the sweep circle expands, the intersections I and I' move along the bisector and away from P, meaning exactly one of them reaches V eventually. More precisely, the following lemma captures from which directions the intersections approach a Voronoi vertex. Recall that $\sphericalangle ABC$ denotes the angle between $\overrightarrow{BA}$ and $\overrightarrow{BC}$ in clockwise direction around B.

▶ **Lemma 10.** *Let $V \in \mathcal{V}$ be a Voronoi vertex with far point V' and incidence tuple (S_1, S_2, S_3). Further, let $(S, S') \in \{(S_1, S_2), (S_2, S_3), (S_1, S_3)\}$, let $\overrightarrow{V}$ be the angular bisector of $\sphericalangle SVS'$, and let $I \in \partial S \cap \partial S'$ be the intersection with $I = V$ at $\hat{r} = r(V')$. Then, $I \in \overrightarrow{V}$ for $\hat{r} < r(V')$.*

Proof. Note that V divides $S \perp S'$ into the two rays $\overrightarrow{V}$ and $S \perp S' \setminus \overrightarrow{V}$ and so does the line $\overleftrightarrow{OV}$. Thus, since $I \in S \perp S'$, it suffices to show that I and $\overrightarrow{V}$ are on the same side of $\overleftrightarrow{OV}$. Without loss of generality, assume $r(S) \geq r(S')$. By Lemma 9 there is a point $P = \overline{OS} \cap S \perp S'$ such that $I \in \overline{PV} \subset S \perp S'$. Thus, P and I are on the same side of $\overleftrightarrow{OV}$. Moreover, since $P \in \overline{OS}$, we also know that S and I are on the same side of $\overleftrightarrow{OV}$. Consequently, it suffices to show that $\overrightarrow{V}$ is on the same side of $\overleftrightarrow{OV}$ as S, as shown in Figure 9.

If S' is on the same side of $\overleftrightarrow{OV}$ as S, then this is trivially true, since $\overrightarrow{V}$ is the angular bisector of $\sphericalangle SVS'$. Thus, let S and S' lie on opposite sides of $\overleftrightarrow{OV}$ and consider the angles $\varphi_S = \sphericalangle SVO$ and $\varphi_{S'} = \sphericalangle OVS'$. Since $\overrightarrow{V}$ is the angle bisector of $\sphericalangle SVS'$, we know that the angle between $\overrightarrow{VS}$ and $\overrightarrow{V}$ is $1/2(\varphi_S + \varphi_{S'})$. To show that $\overrightarrow{V}$ is on the same side of $\overleftrightarrow{OV}$ as S,

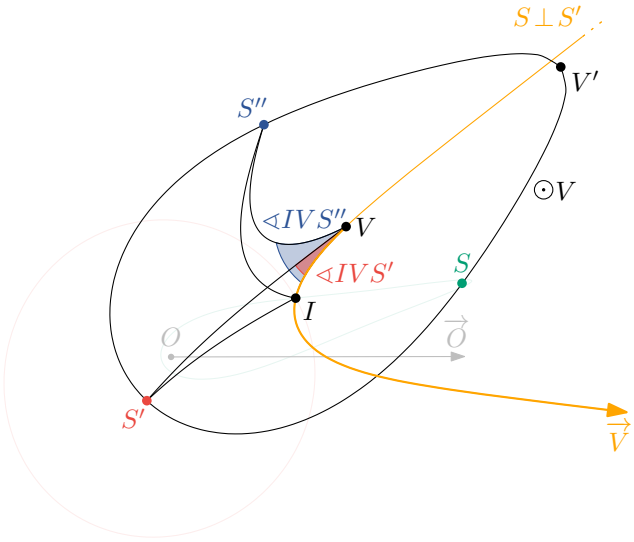


Figure 10 Illustration of Corollary 11. The distance from I to S' is smaller than the one to S''.

it then suffices to show that $1/2(\varphi_S + \varphi_{S'}) \leq \varphi_S$ or equivalently that $\varphi_{S'} \leq \varphi_S$. To this end, we make use of the hyperbolic law of cosines.

Consider the triangles $\triangle OVS$ and $\triangle OVS'$ and note that φ_S and $\varphi_{S'}$ are the angles at V, respectively. Moreover, since S and S' lie on the witness circle of V, we have $|\overline{VS}| = |\overline{VS'}|$. If $r(S') = r(S)$, the side lengths of the triangles match and we have $\varphi_S = \varphi_{S'}$ by Equation (1). If $r(S') < r(S)$, i.e., if $|\overline{OS'}| < |\overline{OS}|$, we can apply Lemma 1 to conclude that $\varphi_{S'} < \varphi_S$. ◀

As a corollary of the above lemma, we can conclude that before the sweep circle radius reaches the far point V' of V, there are two intersections whose distance to the sites of the intersecting beach ellipses is smaller than to the third site, as shown in Figure 10.

▶ **Corollary 11.** *Let $V \in \mathcal{V}$ be a Voronoi vertex with far point V' and incidence tuple (S_1, S_2, S_3). Further, let $(S, S', S'') \in \{(S_1, S_2, S_3), (S_2, S_3, S_1)\}$ and consider the intersection $I \in \partial S \cap \partial S'$ with $I = V$ at $\hat{r} = r(V')$. Then, $|\overline{IS''}| > |\overline{IS}| = |\overline{IS'}|$ for $\hat{r} < r(V')$.*

Proof. Without loss of generality, assume that $\sphericalangle S'VS'' \leq \sphericalangle S''VS$. Consider the two triangles $\triangle IVS'$ and $\triangle IVS''$, as illustrated in Figure 10, and note that $|\overline{VS'}| = |\overline{VS''}|$, since S' and S'' lie on the witness circle of V. By Lemma 10, we know that I lies on the angle bisector $\vec{V}$ of $\sphericalangle SVS'$, meaning I lies between $\overrightarrow{VS}$ and $\overrightarrow{VS'}$ in clockwise direction around V. By definition of the incidence tuple, we know that S'' does not lie between $\overrightarrow{VS}$ and $\overrightarrow{VS'}$ in clockwise direction, meaning $\sphericalangle IVS' < \sphericalangle IVS''$. Consequently, we can apply Lemma 1 to conclude that $|\overline{IS}| = |\overline{IS'}| < |\overline{IS''}|$. ◀

Finally, we investigate how we can use the beach ellipse intersections to predict circle events and how to distinguish between true and false ones (see Section 3.2). Predicting the event is straightforward, as we only need to compute the intersection P of the two bisectors corresponding to two beach ellipse intersections that are consecutive[4] on the beach curve. We note that P may not exist, in which case no circle event is predicted. If it does exist, we need to determine whether the two beach ellipse intersections converge towards P as the

[4] We argue in the proof of Lemma 18 that it suffices to consider consecutive intersections.

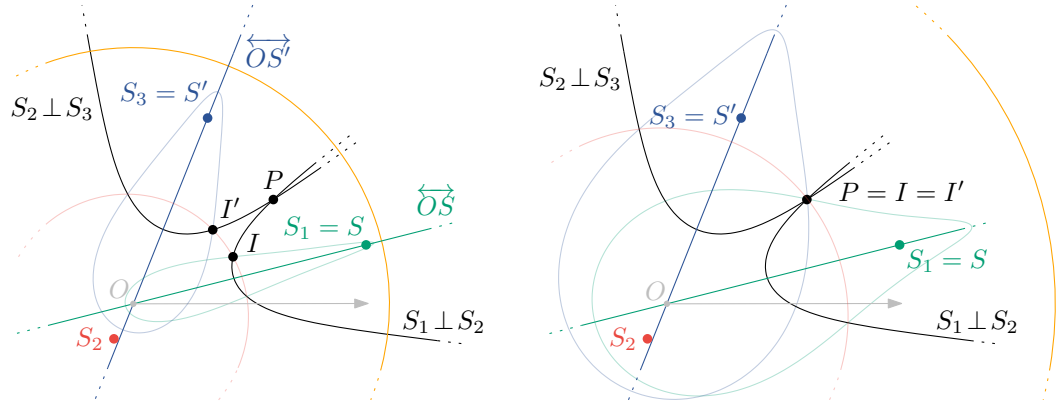


Figure 11 Illustration of Lemma 12. **(Left)** The sweep circle (orange) has radius $\hat{r} < r(P) + d$. The point P and the intersections I and I' are on the same sides of $\overleftrightarrow{OS}$ and $\overleftrightarrow{OS'}$, respectively. **(Right)** The intersections meet at P when $\hat{r} = r(P) + d$.

sweep circle expands. To this end, let S_1 and S_2 be two sites and recall that an intersection $I \in \partial S_1 \cap \partial S_2$ moves away from the line through the pole and the site with the larger radius (Lemma 9). We call this site the *dominant site* of I. The following lemma now says that, as the sweep circle expands, two beach ellipse intersections meet at a point P (predicting a true circle event), if P and the intersections are on the same side of the lines through the pole and the dominant sites. See Figure 11 for an illustration.

▶ **Lemma 12.** *Let $S_1, S_2, S_3 \in \mathcal{S}_{\leq \hat{r}}$ be distinct and let $P \in \mathbb{H}^2$ lie at distance d to them. Further, let $r < r(P) + d$ be such that $I \in \partial S_1 \cap \partial S_2$ and $I' \in \partial S_2 \cap \partial S_3$ are distinct at $\hat{r} = r$ and let S and S' be their dominant sites, respectively. Then, $P = I = I'$ at $\hat{r} = r(P) + d$, if and only if P and I (resp. I') are on the same side of $\overleftrightarrow{OS}$ (resp. $\overleftrightarrow{OS'}$) at $\hat{r} = r$.*

Proof. We give the proof for I and $\overleftrightarrow{OS}$. The one for I' and $\overleftrightarrow{OS'}$ is analogous. Note that the positions of the sites and thus the coordinates of S and P are fixed. Consequently, P is on the same side of $\overleftrightarrow{OS}$ at all times. Moreover, by Lemma 9 the intersection I is on the same side of $\overleftrightarrow{OS}$ at all times. It follows that, if and only if P and I are on the same side of $\overleftrightarrow{OS}$ at a given sweep circle radius, then this holds for all sweep circle radii.

When $\hat{r} = r(P) + d$, the sweep circle has equal distance to P as to all sites S_1, S_2, and S_3, meaning P lies on their beach ellipses. In particular, we have $P = I$. Clearly, P and I lie on the same side of $\overleftrightarrow{OS}$ at that point. By the above argumentation, then and only then does the same hold at $\hat{r} = r$. ◀

A.3.2 Active Beach Ellipse Segments

In this section, we consider how the beach curve changes as the sweep circle expands. We start by proving the following lemma, which characterizes when beach ellipse intersections are active, i.e., when they are on the beach curve $\mathcal{B}$, as depicted in Figure 12.

▶ **Lemma 13.** *Let $S, T \in \mathcal{S}_{\leq \hat{r}}$ be two sites and let $I \in \partial S \cap \partial T$ be an intersection of their ellipses. Then, $I \in \mathcal{B}$ if and only if there exists no site $S' \in \mathcal{S}_{\leq \hat{r}}$ with $S' \neq S, T$ such that $|\overline{S'I}| < |\overline{SI}| = |\overline{TI}|$.*

Proof. We start by proving that S' does not exist if $I \in \mathcal{B}$. To this end, we show for each $S' \in \mathcal{S}_{\leq \hat{r}}$ with $S' \neq S, T$, that $|\overline{S'I}| \geq |\overline{SI}| = |\overline{TI}|$. Consider the intersection $P \in \overrightarrow{OI} \cap \partial S'$.

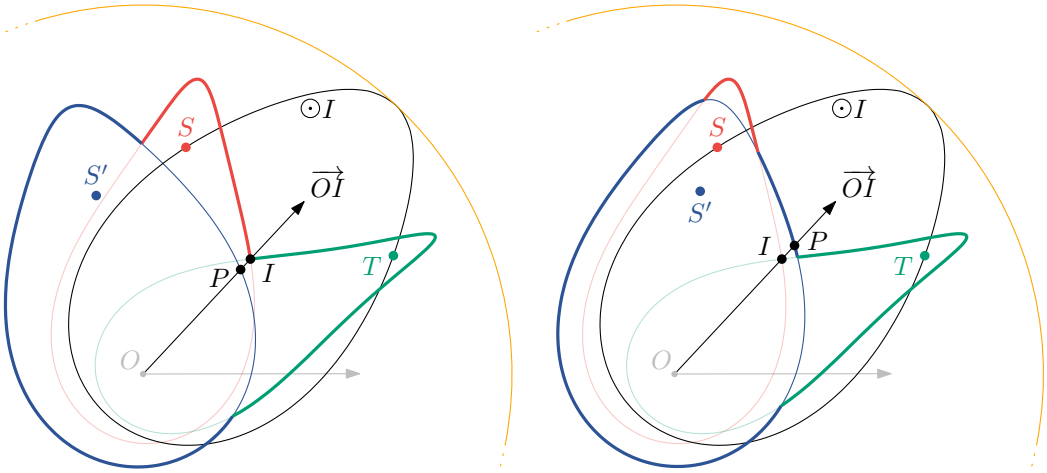


Figure 12 Illustration of the proof of Lemma 13. The circle $\odot I$ contains all points that lie at equal distance to I as S and T. Note that this circle is tangent to the sweep circle (orange). **(Left)** The intersection I is on the beach curve (bold), since S and T are closer to I than S'. **(Right)** The intersection I is not on the beach curve, since S' is closer to I than S and T

Since $I \in \mathcal{B}$, we know that $r(I) \geq r(P)$, meaning I is not inside the beach ellipse $\mathcal{O}S'$. Thus, I is at least as close to the sweep circle as to S'. Since the distance between I and the sweep circle is given by $\hat{r} - r(I)$, it follows that $|\overline{S'I}| \geq \hat{r} - r(I) = |\overline{SI}| = |\overline{TI}|$.

It remains to consider the case where $I \notin \mathcal{B}$. Then, there exists a beach ellipse segment of another site $S' \neq S, T$ that is active at angular coordinate $\varphi(I)$. That is, there is a point $P = \overrightarrow{OI} \cap \mathcal{O}S'$ such that $r(I) < r(P)$. It follows that I is inside of $\mathcal{O}S'$, meaning I is closer to S' than to the sweep circle. We can conclude that $|\overline{S'I}| < \hat{r} - r(I) = |\overline{SI}| = |\overline{TI}|$. ◀

With the above lemma, we are now ready to investigate how changes to the beach curve are related to the events in the queue $\mathcal{Q}$. Consider the tuple $\bar{\mathcal{Q}}$ containing all site events and all true circle events (see Section 3.2). Recall that V' denotes the far point of a Voronoi vertex V, i.e., the point with the maximum radial coordinate among points on the witness circle of V. Then, $\bar{\mathcal{Q}} = (r_0, r_1, \ldots, r_k, r_{k+1})$ contains the radii $r_0 = 0$, $r_{k+1} = \infty$ and all radii $\{r(S) \mid S \in \mathcal{S}\} \cup \{r(V') \mid V \in \mathcal{V}\}$ in ascending order inbetween. We note that $\bar{\mathcal{Q}}$ is different from $\mathcal{Q}$, since the latter also contains structure events and circle events that are later canceled, e.g., when a site is detected within the corresponding witness circle.

For two sites $S, T \in \mathcal{S}_{\leq \hat{r}}$, we say that a point $P \in \mathcal{O}S \cap \mathcal{O}T$ *enters the beach curve at radius* r, if there is an $\varepsilon > 0$ such that $P \notin \mathcal{B}$ for $\hat{r} \in [r - \varepsilon, r)$ and $P \in \mathcal{B}$ when $\hat{r} = r$. Analogously, we say that $P \in \mathcal{O}S \cap \mathcal{O}T$ *leaves the beach curve at radius* r if $P \in \mathcal{B}$ when $\hat{r} = r$ and there is an $\varepsilon > 0$ such that $P \notin \mathcal{B}$ for $\hat{r} \in (r, r + \varepsilon]$. In the following, we show that no beach ellipse intersection enters or leaves the beach curve between two events in $\bar{\mathcal{Q}}$.

▶ **Lemma 14.** *Let $\bar{\mathcal{Q}}$ be the tuple of site events and true circle events and let $r_i, r_j \in \bar{\mathcal{Q}}$ be two consecutive events. Then, for all $\hat{r} \in (r_i, r_j)$ no beach ellipse intersection enters the beach curve.*

Proof. Let S, T be two sites and let $I \in \mathcal{O}S \cap \mathcal{O}T$ be an intersection of their ellipses. For the sake of contradiction, assume that there exists an $r \in (r_i, r_j)$ such that I enters the beach curve at r. Note that no site event occurs in (r_i, r_j), since this would contradict the construction of $\bar{\mathcal{Q}}$. Consequently, if I is on the beach curve at $\hat{r} = r$, we know that I is

contained in the sweep circle for all $\hat{r} \in (r_i, r_j)$. By Lemma 13 we know that I not being on the beach curve before $\hat{r} = r$ implies the existence of at least one site $S' \neq S, T$, such that $|\overline{S'I}| < |\overline{SI}| = |\overline{TI}|$. In particular, we choose S' to be the one that remains active the longest at angular coordinate $\varphi(I)$ as the sweep circle expands beyond r_i. Since I is on the beach curve at $\hat{r} = r$, we also know that $|\overline{S'I}| \geq |\overline{SI}| = |\overline{TI}|$ at that moment (again Lemma 13). Thus, as I moves along the bisector $S \perp T$, there exists an $r' \in (r_i, r]$ such that $|\overline{S'I}| = |\overline{SI}| = |\overline{TI}|$ (Lemma 2). Then, I is the center of an empty circle (as otherwise there would be yet another site that is longer active than S', contradicting the choice of S') and thus lies on a Voronoi vertex $V \in \mathcal{V}$. However, this would imply that $r' \in (r_i, r_j)$ is the radius of the far point of V, which again contradicts the construction of $\bar{\mathcal{Q}}$. ◀

Note that if no intersections enter the beach curve between events in $\bar{\mathcal{Q}}$, then also no beach ellipse segments can become active then. Moreover, no segments become active during a circle event either, as only two intersections are merged into one there. We can conclude the following lemma, which is the hyperbolic sweep circle counterpart of [11, Lemma 7.6] in the Euclidean sweep line version.

▶ **Lemma 15.** *The only way in which a new beach ellipse segment can become active is through a site event.*

We continue by investigating how beach ellipse segments disappear from the beach curve. Analogous to the proof of Lemma 14, we can prove that no beach ellipse intersection leaves the beach curve between two events in $\bar{\mathcal{Q}}$.

▶ **Lemma 16.** *Let $\bar{\mathcal{Q}}$ be the tuple of site events and true circle events and let $r_i, r_j \in \bar{\mathcal{Q}}$ be two consecutive events. Then, for all $\hat{r} \in (r_i, r_j)$ no beach ellipse intersection leaves the beach curve.*

Proof. Consider two sites S, T, let $I \in \partial S \cap \partial T$ be an intersection of their ellipses, and assume for the sake of contradiction that there exists an $r \in (r_i, r_j)$ such that I leaves the beach curve at r. That is, there exists an $\varepsilon > 0$, such that I is on the beach curve until $\hat{r} = r$ and is no longer on the beach curve for $\hat{r} \in (r, r + \varepsilon)$. By Lemma 13, it follows that for all sites $S' \neq S, T$ we have $|\overline{S'I}| \geq |\overline{SI}| = |\overline{TI}|$ at $\hat{r} = r$, but at least one of them is closer to I than $|\overline{SI}| = |\overline{TI}|$ afterwards. Let S'' be the one for which this happens first. That is, for this site we have $|\overline{S''I}| \geq |\overline{SI}| = |\overline{TI}|$ at $\hat{r} = r$ and $|\overline{S''I}| < |\overline{SI}| = |\overline{ST}|$ afterwards. By Lemma 2, we know that when I moves along the bisector $S \perp T$ as the sweep circle expands, there exists a radius $r' \in [r, r + \varepsilon)$ such that $|\overline{S''I}| = |\overline{SI}| = |\overline{TI}|$ when $\hat{r} = r'$. As by the choice of S'', no other site is closer to I than S'', S, and T, we know that I is the center of an empty circle and thus lies on a Voronoi vertex $V \in \mathcal{V}$. However, this implies that $r' \in (r_i, r_j)$ is the radius of the far point of V, which contradicts the construction of $\bar{\mathcal{Q}}$. ◀

Again, note that if no intersections can leave the beach curve between events in $\bar{\mathcal{Q}}$, then also no beach ellipse segment can become inactive then. Moreover, no segments become inactive during a site event, since we only insert two intersections consecutively on the beach curve there. As a result, we obtain the following lemma, which is the hyperbolic equivalent of [11, Lemma 7.7] in the Euclidean sweep line approach.

▶ **Lemma 17.** *The only way in which an active beach ellipse segment can become inactive is through a circle event.*

A.3.3 Voronoi Vertices

It remains to prove that all Voronoi vertices are actually found by means of circle events. The following lemma is the analog of [11, Lemma 7.8] in the Euclidean version. To simplify the following proof, we assume that at most three sites are incident to a Voronoi vertex V. If this does not hold, the algorithm may produce duplicate Voronoi vertices, which need to be merged in a post-processing step.

▶ **Lemma 18.** *Every Voronoi vertex is detected by means of a circle event.*

Proof. Let $V \in \mathcal{V}$ be a Voronoi vertex, let V' be its far point, and let (S_1, S_2, S_3) be the incidence tuple of V. Further, let $r \in \bar{\mathcal{Q}}$ be the predecessor of $r(V')$ in $\bar{\mathcal{Q}}$. We prove that for all sweep circle radii $\hat{r} \in [r, r(V'))$ there are beach ellipse intersections $I_{12} \in \partial S_1 \cap \partial S_2$ and $I_{23} \in \partial S_2 \cap \partial S_3$ that are consecutive on the beach curve $\mathcal{B}$. Then, it follows that the corresponding circle event is in $\mathcal{Q}$ and the Voronoi vertex V is detected at $\hat{r} = r(V')$.

We start by showing that $I_{12}, I_{23} \in \mathcal{B}$ for $\hat{r} \in [r, r(V'))$. In particular, we give the proof for I_{12}, as the one for I_{23} is analogous. For the sake of contradiction, assume that there exists an $r' \in [r, r(V'))$ such that $I_{12} \notin \mathcal{B}$ when $\hat{r} = r'$. By Lemma 7, I_{12} exists, so the only way for it *not* to be on the beach curve is that there exists another site $S \neq S_1, S_2$ such that $|\overline{SI_{12}}| < |\overline{S_1 I_{12}}| = |\overline{S_2 I_{12}}|$ (Lemma 13). Moreover, by Corollary 11 we have $|\overline{S_3 I_{12}}| > |\overline{S_1 I_{12}}| = |\overline{S_1 I_{12}}|$. It follows that $S \neq S_3$. We now show that the site S that is distinct from S_1, S_2, and S_3 cannot exist.

By Lemma 14 we know that I_{12} does not enter the beach curve until at least $\hat{r} = r(V')$. Now first consider the case where I_{12} enters the beach curve exactly at $\hat{r} = r(V')$, i.e., exactly when $I_{12} = V$. This means that $|\overline{SI_{12}}| \geq |\overline{S_1 I_{12}}| = |\overline{S_2 I_{12}}|$ at this point (Lemma 13). In particular, we have $|\overline{SI_{12}}| = |\overline{S_1 I_{12}}| = |\overline{S_2 I_{12}}|$ then, as by Lemma 2 there exists a point at which we have equality but this point does not occur before $\hat{r} = r(V')$. It follows that besides S_1, S_2, and S_3, the site S is on the witness circle of V, contradicting our assumption that no more than three sites do. Now consider the case where I_{12} does not enter the beach curve at $\hat{r} = r(V')$, i.e., when $I_{12} = V$. By Lemma 13, we know that $|\overline{SI_{12}}| < |\overline{S_1 I_{12}}|$, i.e, $|\overline{SV}| < |\overline{S_1 V}|$, which means that S is contained in the witness circle of V, contradicting the assumption that V is a Voronoi vertex. Since both cases lead to a contradiction, we can conclude that $I_{12} \in \mathcal{B}$ for all $\hat{r} \in [r, r(V'))$.

It remains to show that I_{12} and I_{23} are also consecutive on $\mathcal{B}$ for $\hat{r} \in [r, r(V'))$. First note that any intersection that were to lie between I_{12} and I_{23} cannot span beyond these two intersections, as this would contradict the fact that $I_{12}, I_{23} \in \mathcal{B}$, which we just proved. It follows that if I_{12}, I_{23} are not consecutive on $\mathcal{B}$, then there are at least two intersections I and I' between them that belong to the same active segment $\mathcal{A}$, which is part of the beach ellipse of another site S. Since none of the intersections I_{12}, I_{23}, I, and I' leave $\mathcal{B}$ until at least $\hat{r} = r(V')$ (Lemma 16), it follows that I and I' stay between I_{12} and I_{23} until $\hat{r} = r(V')$, which is when I_{12} and I_{23} meet at V. Then, $V = I_{12} = I_{23} = I = I'$. Now note that only three intersections of the beach ellipses of the sites S_1, S_2, and S_3 meet at V, since the two beach ellipse intersections of a pair of them travel in opposite directions on the perpendicular bisector, only one of which leads to V (Lemma 9). Thus, at least one of I and I' belongs to a beach ellipse ∂S with $S \neq S_1, S_2, S_3$. It follows that a fourth site lies on the witness circle of V, contradicting the assumption that no more than three do. ◀

A.4 Complexity

To conclude the proof of Theorem 5, it remains to show that the algorithm takes time $\mathcal{O}(n \log(n))$ to compute the Voronoi diagram of n sites. Initially, all site events need to be

scheduled, meaning the sites have to be sorted by their radii, which takes time $\mathcal{O}(n \log(n))$. The running time of the remainder of the algorithm then depends on the complexity of the diagram, i.e., the number of Voronoi vertices and edges. It was previously shown that this complexity is $\mathcal{O}(n)$, by examining different models: the Poincare disk model [6, Consequence of Proposition 2], the Poincaré half-plane model [10, Theorem 18.5.1] and the Klein disk model [27, Theorem 1]. Of course, it is no surprise that all came to the same conclusion, since the different models represent different ways to address points in the same space.

Clearly, there are exactly n site events and the number of true circle events is bounded by the number of Voronoi vertices, which is $\mathcal{O}(n)$. As each event is processed, at most a constant number of circle events are scheduled and as the algorithm proceeds the number of canceled events cannot be larger than the scheduled ones. Moreover, since each intersection can contribute at most one structure event, it follows that the total number of processed events is $\mathcal{O}(n)$.

It remains to show that we can handle an event in time $\mathcal{O}(\log(n))$. Since the queue contains $\mathcal{O}(n)$ events, inserting and removing elements from the queue, takes time $\mathcal{O}(\log(n))$. Regarding updating the beach curve data structure, recall that two beach ellipses intersect at most two times (Lemma 7) and note that, consequently, at most two intersections are on the same edge of the Voronoi diagram at all times. It follows that the number of elements in the beach curve is at most $\mathcal{O}(n)$ at all times, meaning insertions and deletions take at most $\mathcal{O}(\log(n))$ time. All other operations, like inserting vertices to the diagram, marking bisectors incident to the vertices, and predicting new circle and structure events, take constant time.